

Water Resources Research®

RESEARCH ARTICLE

10.1029/2023WR036769

Key Points:

- Two distinct styles of groundwater response to atmospheric rivers and drought occur in coastal valley aquifers
- Meltwater transported via the Fraser River to the coast mediates drought in hydraulically connected aquifers
- Groundwater memory reflects the signal superposition of physical processes, including the effects of physical boundary conditions

Supporting Information:

Supporting Information may be found in the online version of this article.

Correspondence to:

D. M. Allen,
dallen@sfu.ca

Citation:

Nott, A. H., Allen, D. M., & Hahm, W. J. (2024). Groundwater responses to deluge and drought in the Fraser Valley, Pacific Northwest. *Water Resources Research*, 60, e2023WR036769. <https://doi.org/10.1029/2023WR036769>

Received 23 NOV 2023

Accepted 11 OCT 2024

Groundwater Responses to Deluge and Drought in the Fraser Valley, Pacific Northwest



A. H. Nott¹ , D. M. Allen¹ , and W. J. Hahm² 

¹Department of Earth Sciences, Simon Fraser University, Burnaby, BC, Canada, ²Geography Department, Simon Fraser University, Burnaby, BC, Canada

Abstract Groundwater level variations represent signals of superimposed physical processes, with memory. Groundwater level records are used to understand how aquifer systems respond to natural and anthropogenic perturbations. Here we analyze groundwater levels across the South Coast of British Columbia (BC) in the Pacific Northwest with the objective of determining groundwater responses to atmospheric rivers (ARs) and drought. An AR catalog was derived and used to associate precipitation amounts to AR occurrence. Droughts were quantified using dry day metrics, in conjunction with the standardized precipitation index. Historically (1980–2023), from September to January, approximately 40% of total precipitation was contributed by ARs. From April to September, more than 50% of days received no precipitation, with typically 26 consecutive dry days. We used the autocorrelation structure of groundwater levels, commonly used to characterize aquifer memory, to identify two distinct clusters of observation well responses. Cluster 1 wells respond to recharge from local precipitation, primarily rainfall, and respond rapidly to both ARs during winter recharge and significant rainfall deficits during summer. Cluster 2 wells are driven by local precipitation but are influenced by the Fraser River's large summer freshet which briefly recharges the aquifers, thereby delaying drought propagation. The results suggest that groundwater memory encapsulates multiple hydrogeological factors, including boundary conditions, influencing the response outcome to extreme events.

Plain Language Summary Heavy rainfall events and drought are becoming more commonplace around the world. Their effects are immediately observable to us; we see the devastating impacts of floods and the drying of riverbeds. But what happens in subsurface groundwater systems? We combined real world observation data on groundwater levels, rainfall, and streamflow within the Pacific Northwest to determine groundwater response to heavy rainfall events and drought. We found that aquifers connected to a large river that carries summer snowmelt are more resilient to drought than unconnected aquifers. However, both aquifer groups still depend on heavy rainfall events to recover from drought. As we continue to rely on groundwater for crop irrigation and clean drinking water, climate change will challenge how we manage this resource.

1. Introduction

Groundwater level variations are composite signals that represent the complex superposition of natural and anthropogenic signals, transformed and filtered by various physical processes. Recharge begins as an unaltered signal at the surface, governed by interactions between spatiotemporal variations in climatology (e.g., weather patterns, rainfall intensity) and subsurface characteristics (e.g., vadose zone and saturated zone hydraulic properties) (de Vries & Simmers, 2002; Fetter & Kreamer, 2021). Superimposed onto this recharge signal are processes such as ocean tides (Abarca et al., 2013; Ataie-Ashtiani et al., 2001; Mao et al., 2006), pumping (Barlow & Leake, 2012; Bierkens & Wada, 2019), aquifer-stream interactions (Winter, 1999; Woessner, 2000), barometric and Earth tides (McMillan et al., 2019; Toll & Rasmussen, 2007), evapotranspiration (Condon & Maxwell, 2019; Lautz, 2008), and even seismicity (Barberio et al., 2020).

In the context of signals, groundwater is often considered as possessing memory (Brooks et al., 2021; Duvert et al., 2015; Jukić & Denić-Jukić, 2004; Mangin, 1984), defined here as the responsiveness of the groundwater signal to external inputs, generally recharge, characterizing the degree of propagation delay from the input source. The concept of memory in groundwater research stems from the theory of long-range persistence, which refers to how past states influence or persist into future states of a system (Witt & Malamud, 2013). Longer memory systems tend to respond more slowly and dissipate a more filtered and attenuated input signal, and vice-versa. Factors controlling memory include aquifer hydraulic properties (Duy et al., 2021; Van Lanen et al., 2013),

© 2024. The Author(s).

This is an open access article under the terms of the Creative Commons Attribution License, which permits use, distribution and reproduction in any medium, provided the original work is properly cited.

recharge signals (Bloomfield & Marchant, 2013) and climate variability (Opie et al., 2020), rates of groundwater discharge (Imagawa et al., 2013), and vadose zone thickness (Schuler et al., 2022). Overall, groundwater memory encodes the collective factors of catchment and hydraulic characteristics, and presumably exerts a first-order control on groundwater response to extreme events.

Extreme precipitation and drought—the dichotomies of recharge—lead to variable responses in groundwater depending on the prior series of recharge events and the hydrogeological context (Nygren et al., 2022; Schuler et al., 2022). Extreme precipitation, usually in the form of rain, can be a critical contributor to groundwater recharge (Corona et al., 2023; Taylor et al., 2013), particularly in arid and semi-arid regions where intense rain events are the only major source of recharge to aquifers (Thomas et al., 2016). The vadose zone is arguably the most important recharge signal filter for extreme precipitation events. Unconfined aquifers can respond to infiltration from within several hours to days (Wittenberg et al., 2019), depending on the vadose zone thickness (Schuler et al., 2022), which acts as a reservoir that can store extreme event water (Corona & Ge, 2022). Coarser vadose zones that receive higher infiltration fluxes, such as in temperate climates, have deeper damping depths, increasing the preservation potential of low-frequency climate mode signals in recharge (Corona et al., 2018). Consistently maintaining a moist vadose zone year-over-year tends to favor groundwater recharge, especially for deeper aquifers (Shao et al., 2018). Gu et al. (2022) show that total precipitation amounts in temperate climates influence groundwater levels more strongly than the duration of any individual event. However, rainfall events that exceed the infiltration capacity of the vadose zone can trigger overland flow, reducing net recharge (Rathay et al., 2018). As changes in the intensity, duration, and frequency of these extreme events reshape global, regional, and local hydrological cycles and landscapes (Gleeson et al., 2020; Meixner et al., 2016; Peterson et al., 2021; Thomas et al., 2016), contextualizing the relevant physical processes that forming any given groundwater signal is key.

At the other end of the spectrum, drought is a complex and multi-faceted process that can affect—and propagate to—different components of the hydrological cycle (e.g., soil moisture, groundwater, streamflow), contingent on the extent and length of sustained meteorological moisture deficits (Van Lanen, 2006; Van Loon, 2015; W. Wang et al., 2016). Increased evapotranspiration tends to accelerate drought propagation as atmospheric moisture demand increases (Teuling et al., 2013), thereby increasing temperatures and establishing a positive feedback loop (Bartusek et al., 2022). During drought, groundwater can provide some buffering capacity in maintaining baseflow to streams, delaying the onset of drought propagation to streamflow (Hellwig et al., 2020).

The effects of extreme precipitation and drought on recharge are often studied separately, with the aim of determining the response or outcome to these events. Particularly in drought research, memory is used as an indicator of groundwater resilience or sensitivity (Nygren et al., 2022; Schuler et al., 2022; Sutanto & Van Lanen, 2022), that can also be applied in the context of rainfall extremes (Duvert et al., 2015; Opie et al., 2020; Sorensen et al., 2021). However, we hypothesize that groundwater memory serves a more useful purpose as a means of understanding the hydrogeological context, providing a means to evaluate the response to extreme events. If we consider external input signals, such as aquifer-stream interactions, from the standpoint of boundary conditions, how do these boundaries affect the memory characteristics of groundwater and the response we observe to extremes? In this study, we examine groundwater levels from 34 observation wells (OW) across the Fraser Valley, at the outlet of the Fraser River Basin in the South Coast Region of British Columbia (BC). This paper aims to evaluate groundwater responses to heavy rainfall, via ARs, and drought, by building a contextual understanding of processes influencing groundwater signals using memory characteristics and clustering.

2. Study Area and Methods

2.1. Study Area

The Fraser Valley extends from Hope to the mouth of the Fraser River at the Strait of Georgia (Figure 1). The valley is bordered to the north by the Coast Mountains and to the southeast by the Cascade Mountains. A key hydrological feature of the Fraser Valley is the Fraser River, which drains the Fraser River Basin (inset map in Figure 1) from its Rocky Mountain headwaters, through the Interior Plateau, and into the Pacific Ocean through the Coast Mountains (Martins et al., 2023). The 1,400 km-long Fraser River is predominantly driven by snow- and glacier melt, with substantial rainfall contribution near the coast, reflecting the collective hydrological input of nearly a third of BC (Déry et al., 2012).

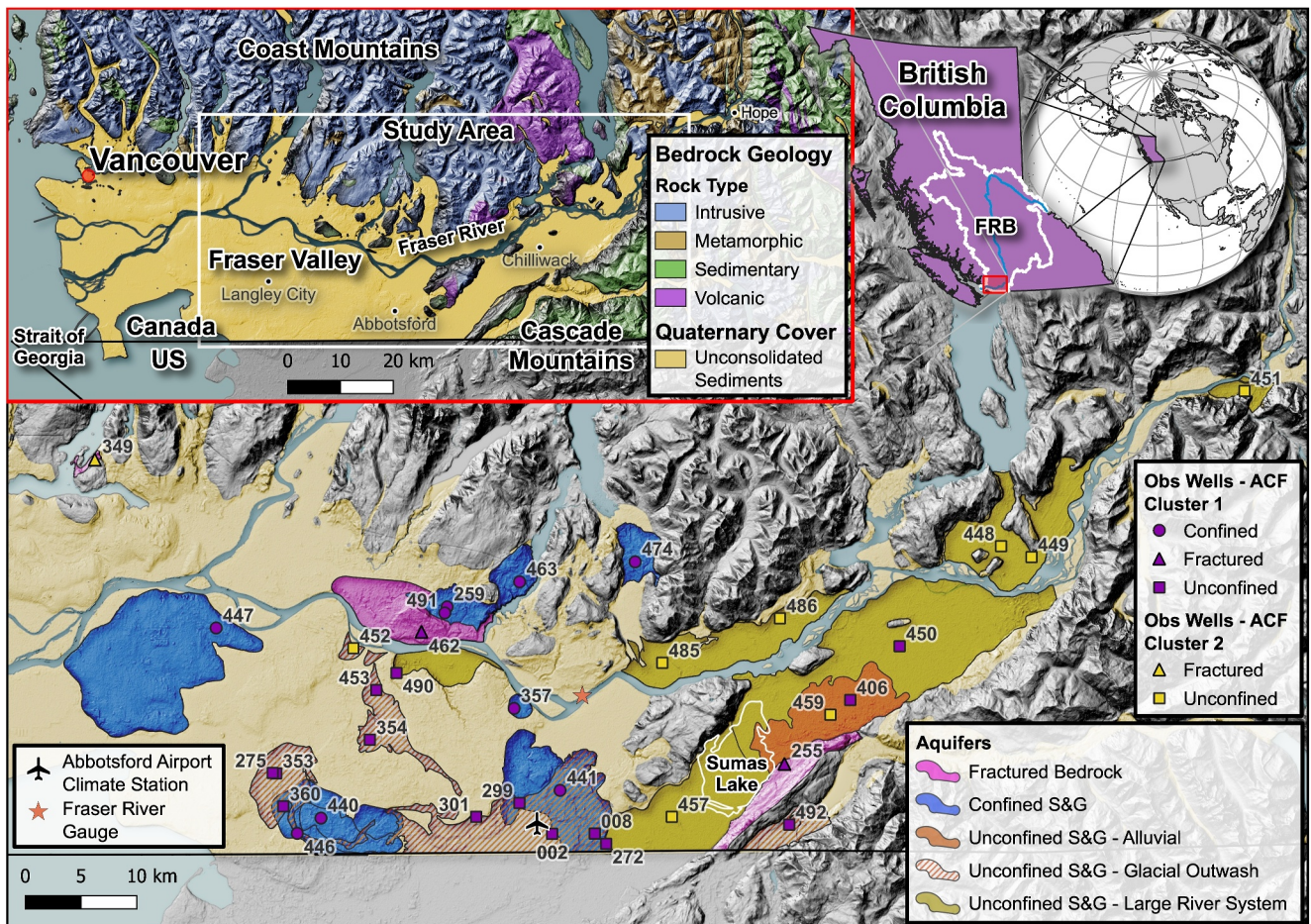


Figure 1. Hydrogeological setting of the Fraser Valley showing the distribution of aquifers (S&G: Sand and Gravel) and observation wells (numbered) along with their associated ACF cluster (see Section 2.5). The Fraser River is the large stream flowing through the valley from east to west. The small provincial inset map shows the Fraser River Basin (FRB) outlined in white with the Fraser River in blue, and the study area is outlined in red. The large inset map shows the underlying bedrock geology (BCGS, 2019) and the extent of unconsolidated fill deposited during the Quaternary. Map created with QGIS v3.26.3 (QGIS Development Team, 2022).

Climate across the Fraser River Basin is diverse, with precipitation ranging from 350 mm/yr (<30% as snow) in the Interior Plateau, to approximately 1,000 mm/yr (>50% as snow) in the Rocky Mountains, and over 3,000 mm/yr (<15% as snow) in the Coast Mountains (Moore et al., 2010). Over much of BC, snow accumulation typically begins in October, peaks in early April, and melts by early August (Curry & Zwiers, 2018). In contrast, the Fraser Valley features a characteristically temperate ocean climate (Köppen-Geiger: *Cfb* bordering *Csb* (Beck et al., 2018)), receiving on average 1,525 mm/yr (range: 1,186–1,994 mm/yr) of precipitation (1991–2020 climate normals). Snowfall constitutes only 3.3%, or 51 mm/yr (range: 8–200 mm/yr), of precipitation. The mean annual temperature is 10.8°C, with summer highs around 25°C, and winter lows just above 0°C (Figure S1 in Supporting Information S1). The Fraser River tends to be event-driven near the coast, where extreme rainfall events can promptly triple the river's discharge (Pawlowski et al., 2017). The Fraser River can exceed 10,000 m³/s during freshet peak flows in late June, while low flows (~1,500 m³/s) persist from December to April (Figure 2b). Peak flows are primarily controlled by the annual maximum snow water equivalent (SWE), and secondarily, by the rate of spring- and summer-time warming (Curry & Zwiers, 2018).

The contemporary physiography of the Fraser Valley is characterized by low relief and gently rolling hills (<150 masl) with isolated bedrock outcrops, bounded by the high relief Coast and Cascade Mountain (Figure 1). This landscape has evolved over hundreds of thousands of years of Quaternary glacial and interglacial processes, largely shaped by the most recent Fraser Glaciation (Clague et al., 1983; Clague & Ward, 2011). Glacio-isostatic adjustment, eustatic sea level change, and successive glacial advances and retreats, have favored the emplacement of a complex succession of alternating marine, glacial, and non-glacial sediments, within the Fraser Valley

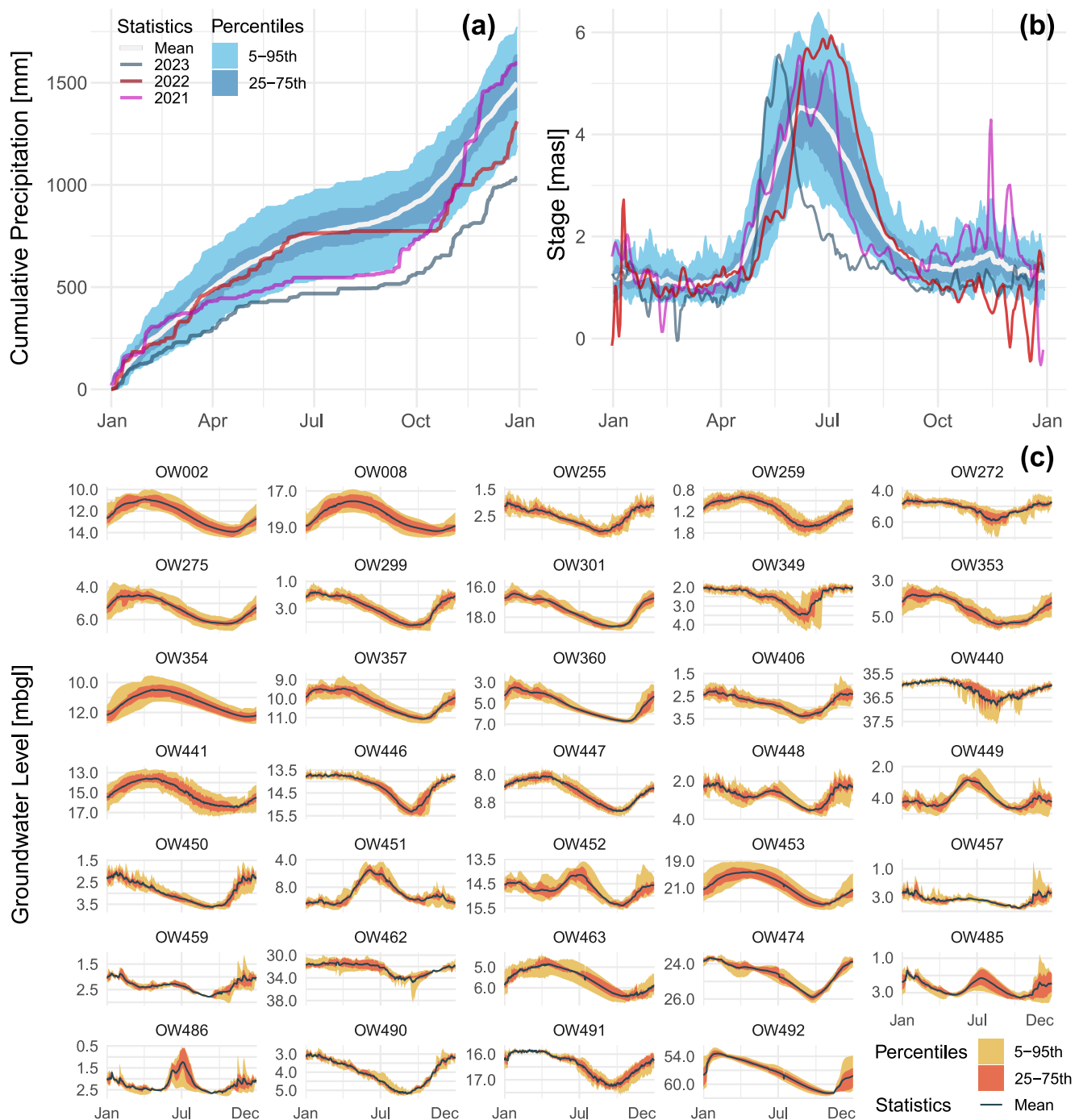


Figure 2. (a) Cumulative precipitation statistics at the Abbotsford Airport Climate Station (EC1100030/31) for the 2020 climate normals period (1991–2020). (b) Fraser River stage statistics (1965–2022) at the Mission hydrometric station (08MH024). (c) Groundwater level hydrographs. See Figure 1 for station and observation well locations.

(Armstrong, 1981; Clague, 1994; Clague & James, 2002). Consequently, the spatial distribution and stratigraphy of aquifers and aquitards within the valley can be quite complex. Aquifers, up to 60 m thick, are predominantly sand and gravel of colluvial, fluvial, and glaciolacustrine origin (Armstrong, 1984). Aquitards, exceeding 80 m of thickness, are predominantly basal and lodgement tills, and clay and silt of marine, lacustrine, glaciomarine, glaciolacustrine, and glacial origin (Armstrong, 1984).

Groundwater levels in aquifers throughout BC are monitored by observation wells (OW) through the Provincial Groundwater Observation Well Network (PGOWN) (BC Ministry of Environment and Climate Change Strategy (ECCS, 2023). We broadly classify aquifers as: fractured bedrock, confined sand and gravel, and unconfined sand and gravel associated with either alluvial, glacial outwash, or large river systems.

2.2. Extreme Events in the Pacific Northwest

Atmospheric rivers are the main mechanism for extreme precipitation events in the Pacific Northwest (Eldardiry et al., 2019; Sharma & Déry, 2020; Tan et al., 2022) and have been an integral component of Western North America's hydrological cycle for at least 600 years (Borkotoky et al., 2023). Atmospheric rivers are prolonged, extensive, and concentrated bands of enhanced water vapor sourced from tropical or extratropical regions (Neiman et al., 2008; Ralph et al., 2018; Zhu & Newell, 1998). While ARs do not always result in extreme precipitation (Collow et al., 2020), they are important drivers of both flooding and—in their absence—drought persistence (Berghuijs & Slater, 2023; Paltan et al., 2017). In mountainous regions, the amount of precipitation contributed from landfalling ARs depends heavily on orographic uplift (Ralph et al., 2016; S. Wang et al., 2023), which causes successive depletion in water vapor, controlling the inland penetration (Tan et al., 2022). Atmospheric rivers are important snowpack building events during the winter at higher altitudes along the North American Cordillera (Eldardiry et al., 2019; Goldenson et al., 2018; Neiman et al., 2008; Paltan et al., 2017; Payne et al., 2020). Although, in the coastal Pacific Northwest, higher AR frequency is associated with lower seasonal snowpacks (Goldenson et al., 2018). Moreover, as ARs are transported via warmer moisture circulations, lower elevations coastal catchments can be subject to substantial snowmelt and rain-on-snow events (Chen et al., 2019; Eldardiry et al., 2019; Guan et al., 2016; Siirila-Woodburn et al., 2023; Spry et al., 2014).

In the Pacific Northwest, drought onset and intensity have increased (Iglesias et al., 2022; Kormos et al., 2016) with a decrease in summer baseflow contributions (Murray et al., 2023). Berghuijs et al. (2022) show that climatic aridity imparts a first-order control on whether precipitation recharges groundwater. Notably, the decline in overall precipitation, and winter precipitation arriving as snow, under a warming climate is expected to significantly affect mountain system recharge (Meixner et al., 2016). This is particularly concerning for coastal catchments that oscillate above and below the freezing point both diurnally and seasonally. Coastal groundwater systems relying on snowpack melt for recharge and baseflow supply during summers face heightened risk (Islam et al., 2017; Mote et al., 2005), which is well documented in the mountainous regions of the Pacific Northwest (Dierauer et al., 2018; Gullacher et al., 2023).

The El Niño–Southern Oscillation (ENSO) is the main driver of interannual precipitation variability in the Pacific Northwest, with less impactful effects from the Pacific Decadal Oscillation (PDO) (Brigode et al., 2013; Fleming & Whitfield, 2010; Lopez & Kirtman, 2019). ENSO can influence extreme precipitation (Brigode et al., 2013) and drought occurrence across the Pacific Northwest (Vicente-Serrano et al., 2011). During an El Niño, the subtropical jet stream strengthens and shifts equatorward (Payne & Magnusdottir, 2014; Seager et al., 2005), causing the Pacific Northwest to be relatively dry and warm during the summer. Additionally, ARs tend to be less frequent during an El Niño summer and winter (Mundhenk et al., 2016). Conversely, the La Niña phase tends to shift storm tracks toward the Pacific Northwest, increasing winter precipitation (Fleming & Whitfield, 2010) at a time when ARs tend to also be more frequent (Mundhenk et al., 2016; Xiong & Ren, 2021). Accordingly, these climate teleconnections can significantly influence drought occurrence, and extreme precipitation, which are reflected in the frequency characteristics of groundwater (Malmgren et al., 2022; Rust et al., 2019; Velasco et al., 2017).

2.3. Hydroclimatological Data

AR and integrated vapor transport (IVT) data were obtained from an online catalog (<https://www.earth-systemgrid.org/dataset/ucar.cgd.artmip.tier1.catalogues.rutz.html>) maintained by the Center for Western Weather and Water Extremes (CW3E), following the AR detection algorithm described in Rutz et al. (2014). The algorithm constraints for AR detection are: atmospheric water vapor feature length $>2,000$ km and IVT $>250 \text{ kg m}^{-1} \text{ s}^{-1}$. This AR catalog, part of the AR Tracking Method Intercomparison Project (ARTMIP) (Rutz et al., 2019), identifies the occurrence (or non-occurrence) of landfalling ARs using MERRA-2 gridded climate reanalysis data (Gelaro et al., 2017). AR detection is sensitive to more complex mountainous topography and has been shown to be best resolved by ERA-5 due to a finer spatial resolution ($0.25^\circ \times 0.25^\circ$) (Collow et al., 2022).

However, the slightly coarser MERRA-2 ($0.5^\circ \times 0.625^\circ$) AR catalog was chosen as it was the most up-to-date catalog (1980–2022). AR data were cropped to an extent of two grid cells (49.0°N , 49.5°N , 121.875°W , 123.125°W) covering the Fraser Valley study region (Figure 1). Then, AR count and mean IVT were converted from three-hourly time steps to daily, if five or more of the eight timesteps were AR occurrences. If an AR was detected in at least one of the grid cells within the study region, then the entire extent was considered to have had an AR occur. Our derived AR counts in the same region compare well (Figure S2 in Supporting Information S1) to both the SIO-R1 AR catalog by Gershunov et al. (2017) and the distribution of landfalling ARs from CW3E (2022).

Climate data (1980–2023) were obtained from the Abbotsford Airport Climate Station (EC1100030/31) (Figure 2a) operated by Environment and Climate Change Canada (ECCC, 2023) and used to associate precipitation amounts to AR occurrence for each day. Based on the coarse spatial resolution of the AR catalog ($\sim 45 \times 56$ km pixels) and the drawbacks of gridded climate data in preserving key features of extreme precipitation (Hu et al., 2018; King et al., 2013; Sun et al., 2018), station-based climate data was deemed appropriate in being able to capture more accurate precipitation associated with ARs, despite the large areal extent of the valley.

Given the relatively short record (~20 years) of daily groundwater data, we chose to focus on ENSO rather than on the PDO, as the latter tends to highlight interdecadal patterns (15-to-25 years) of climate variability (Mantua & Hare, 2002). The Oceanic Niño Index (ONI) is used to identify the positive (El Niño) and negative (La Niña) phases of ENSO (available from the National Oceanic and Atmospheric Administration's (NOAA) Climate Prediction Center CPC, https://origin.cpc.ncep.noaa.gov/products/analysis_monitoring/ensostuff/ONI_v5.php). The ONI is a 3-month running average of sea surface temperature anomalies in the Niño-3.4 region of the Pacific where anomalies above (below) 0.5°C are considered as El Niño (La Niña) events.

2.4. Atmospheric Rivers and Drought Indicators

To investigate the effects of discrete heavy rainfall events, we separated the contribution of AR precipitation to monthly (annual) precipitation by considering the AR fraction of precipitation. The AR fraction was obtained by dividing the total monthly (annual) AR precipitation by the total monthly (annual) precipitation to isolate any distinct effects ARs might have on groundwater levels.

To quantify discrete drought events, we considered two precipitation-based metrics, consecutive dry day (CDD) and number of dry day (NDD). The CDD fraction was computed by taking the longest run of dry days (precipitation < 1 mm) in a month (year) and dividing by the number of days in a month (year). The NDD fraction is simply a count of dry days (precipitation < 1 mm), divided by the number of days in a month (year).

For determining wet and dry periods, the Standardized Precipitation Index (SPI) (McKee et al., 1993) was computed for precipitation at the Abbotsford Airport Climate Station, using the SCI package (Gudmundsson & Stagge, 2016) in R 4.1.3 (R Core Team, 2022). Several accumulation periods for the SPI were explored (3, 6, 9, 12, and 24), but ultimately, an accumulation period of 6 months was chosen to best represent meteorological drought at an appropriate temporal scale (Barker et al., 2016). The Pearson type-3 distribution was used for the SPI (see Figure S3 in Supporting Information S1, for selection choice). Standardized precipitation index values less (more) than -1 ($+1$) represent dry (wet) periods (McKee et al., 1993). Therefore, we used the SPI as a metric of classifying wet or dry (meteorological drought) periods, acting as a measure of antecedent wetness or dryness. Linear regression lines are fit between points for SPI less (more) than -1 ($+1$). This adds more flexibility to exploring groundwater responses in the context of multivariate extremes (Brunner, 2023) over different time scales, where there may be a high CDD or NDD fraction in a positive SPI (wet) period, or conversely, a high AR fraction in a negative SPI (dry) period.

2.5. Hydrogeologic and Hydrometric Data

Streamflow (1965–2023) for the Fraser River at the City of Mission hydrometric station (08MH024) (Figure 2b) was obtained from the Water Survey of Canada (Water Survey of Canada (WSC, 2023)). Hourly (upscaled to daily and monthly) groundwater level data for 34 observation wells (Figure 2c) were obtained from BC's PGOWN (ECCS, 2023). We filtered for well data from 2004 onwards that had at least three years of data (Figure S4 in Supporting Information S1), due to the higher data quality of hourly observations; prior to 2004 groundwater levels were measured monthly. Many of the aquifers in the region—monitored by these wells—support irrigation

and municipal water supplies, with peak usage from June to September. The total licensed amount across the 23 aquifers in this study is approximately 25,415,183 m³/year (BC Ministry of Water, Land and Resource Stewardship (WLRS, 2024), although this amount does not account for pending licenses and unauthorized use (Table S1 in Supporting Information S1). Disentangling the effect of abstraction on drought (AghaKouchak et al., 2021) or extreme precipitation (Sorensen et al., 2021) can be challenging, and is acknowledged in this study as a superimposed signal acting as a potential confounding factor. However, this effect was minimized by removing wells (10 of the 44 across the Fraser Valley) with statistically significant trends, tested using the zyp R package (Bronaugh et al., 2023), pumping patterns, or obvious breakpoints (Table S1 in Supporting Information S1). None of the wells in the Fraser Valley show signs of groundwater depletion preventing the recovery of levels from seasonal recharge, similar to the case in the United Kingdom (Wendt et al., 2020).

Information for aquifers (Table S1 in Supporting Information S1) associated to each observation well was obtained from the mapped aquifer registry (WLRS, 2023). Hydraulic tests have not been performed in the wells, and therefore, transmissivity and storativity values were assigned (Table S1 in Supporting Information S1) as best estimates (for 26 wells) from various pumping tests conducted around the Fraser Valley (Carmichael, 2013; Cox & Kahle, 1999; Gibbons & Culhane, 1994; Golder Associates Ltd, 2005; Piteau Associates Engineering Ltd, 2012; Ricketts, 1998, 2000; Scibek & Allen, 2005). Fractured aquifer transmissivity and storativity were estimated from literature (Kuang et al., 2020) and well completion reports (ECCS, 2023). We used transmissivity, in dimensions of (L²/T), and storativity, dimensionless, to determine the hydraulic diffusivity, the ratio of transmissivity to storativity, in dimensions of (L²/T).

2.6. Memory Metrics and Autocorrelation Clustering

Autocorrelation measures the linear relationship, or degree of similarity, between subsequent values of the same timeseries lagged over time (Maity, 2018). The autocorrelation function (ACF) of groundwater levels has been widely used in the literature to quantify aquifer memory in karst and fractured bedrock systems (Bloomfield & Marchant, 2013; Delbart et al., 2016; Lafare et al., 2016; Mangin, 1984; Massei et al., 2006; Schuler et al., 2020; Sorensen et al., 2021), and porous alluvial systems (Duvert et al., 2015; Duy et al., 2021; Imagawa et al., 2013; Nygren et al., 2022; Schuler et al., 2022). Mangin (1984) used an ACF threshold of 0.2 to extract the decorrelation lag time to quantify this memory effect. Massei et al. (2006) emphasized the importance of considering the shape of the ACF in characterizing memory, by fitting a logarithmic function to the ACF at early lag times, to determine a decay rate. This method is often applied to karst systems (Delbart et al., 2016), but has also been used in alluvial systems (Duvert et al., 2015; Duy et al., 2021). Alternatively, a linear fit, to determine decay (slope), can also be applied to early lag times (Delbart et al., 2016; Imagawa et al., 2013).

We used three different ACF-derived metrics to attempt to quantify aquifer memory (Figure 3, summarized in Table S1 in Supporting Information S1). First, we considered the traditional decorrelation lag time by threshold (ACF = 0.2). Second, we considered the linear decay rate at early lag times (<150 days) by iteratively fitting a straight line to an optimal fit window of lag times (by maximizing the fit R²). Finally, we introduce an approach to characterizing the progressive attenuation of the oscillatory ACF pattern. We fit an exponentially decaying (damped) sinusoid function (lag <1,000 days) to determine a decay rate of the ACF oscillation pattern:

$$y(t) = Ae^{-\lambda t} \cos(\omega t - \varphi) \quad (1)$$

where A is the amplitude (−), λ is the exponential decay rate (T⁻¹), ω is the angular frequency (T⁻¹), and φ is the phase shift (−). See Figures S5, S6, and S7 in Supporting Information S1 for the memory metrics mapped to each well.

Exploring memory characteristics revealed distinct ACF shapes (Figure 3). Agglomerative hierarchical clustering, which performs well with groundwater data (Giese et al., 2020; Yin et al., 2022), was applied to groundwater level ACFs and optimized two clusters. We applied the Ward Linkage method implementing Euclidean distance as the dissimilarity metric, which tends to result in more distinct and homogenous clusters (Haaf & Barthel, 2018). Clustering was performed using the factoextra R package (Kassambara & Mundt, 2020), and the optimal number of clusters was confirmed using the NbClust R package (Charrad et al., 2014).

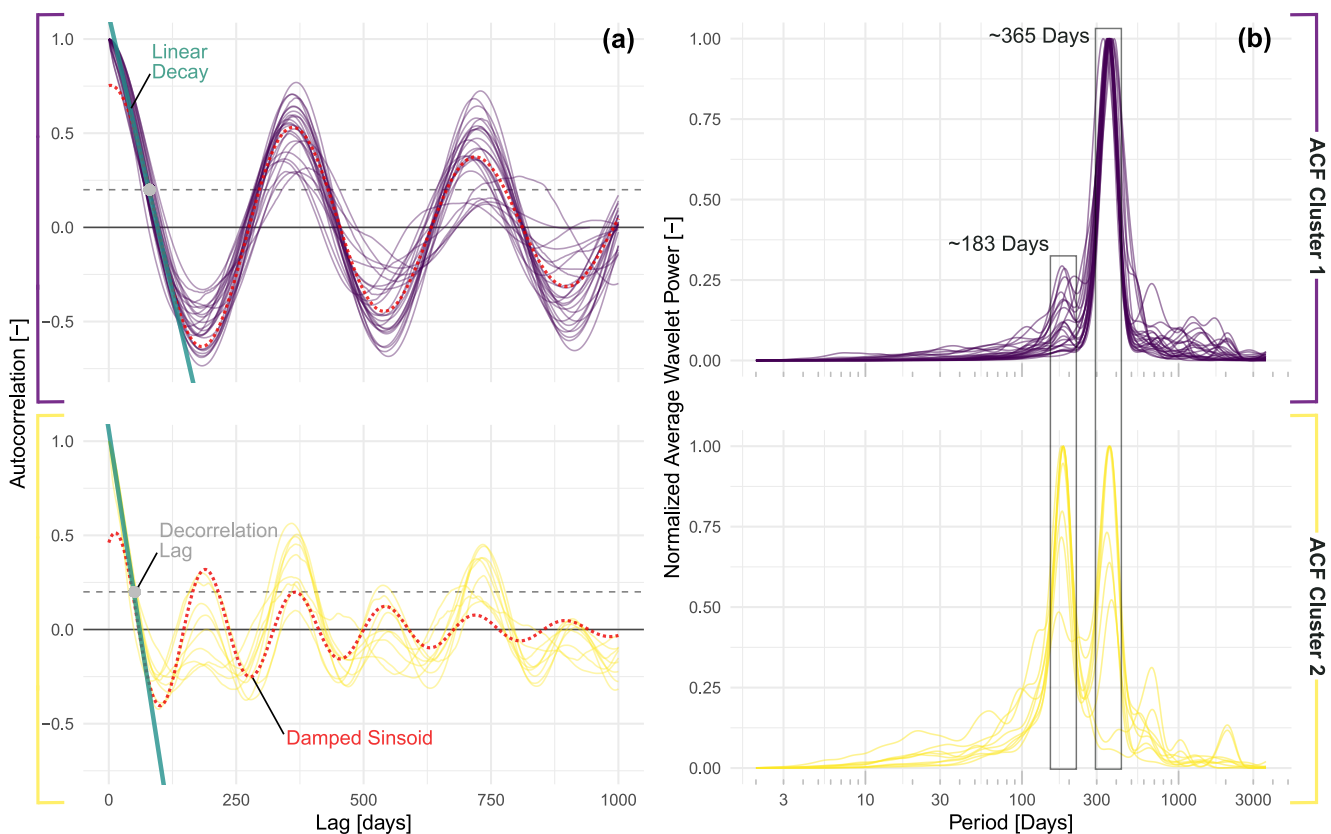


Figure 3. (a) Groundwater ACF clusters and cluster-averaged memory metrics including the linear decay rate, the decorrelation lag time, and the damped sinusoid. (b) Frequency characteristics for each ACF cluster based on the normalized average wavelet power.

2.7. Groundwater Level Adjustments

Groundwater may not immediately respond to ARs or drought. This delay was accounted for by considering a forward lead observation (e.g., considering the following month). Interestingly, groundwater level rates-of-change, by successive differencing, cross-correlated with precipitation rate suggest that in nearly all wells, the initial groundwater response can be on the order of days (Figure S8 in Supporting Information S1). However, groundwater level cross-correlated with precipitation reveals that the full response, or total amount of recharge from a precipitation event, is differentially delayed on the order of months (Figure S9 in Supporting Information S1). To determine an appropriate lead time adjustment, we checked the cross-correlation lag time (at maximum correlation) between groundwater levels and precipitation. Lead adjustments range from 2 to 4 months in confined aquifers, 0 to 2 months in fractured aquifers, and 0 to 4 months in unconfined aquifers. Cluster 2 groundwater levels were unadjusted because of aquifer-stream interactions (discussed below). We assume minimal snow storage acting as lagged recharge based on the snowfall fraction.

2.8. Wavelet Analysis

The Continuous Wavelet Transform (CWT) was used to determine time-averaged frequency spectrums (wavelet spectra) for groundwater levels, and SPI, using the WaveletComp R package (Roesch & Schmidbauer, 2018). The wavelet coherence is a measure of coherency (ranging from 0 to 1), or synchronicity in the time-frequency domain, between two signals from the cross-wavelet transform, a time-frequency analogue to cross-correlation (Torrence & Compo, 1998). The CWT and wavelet coherence are advantageous for elucidating changes in frequency over time in non-normal and non-stationary hydrological data (Grinsted et al., 2004; Sang, 2013), and have been effectively applied to groundwater levels (Duvert et al., 2015; Kuss & Gurdak, 2014; Malmgren et al., 2022; Rust et al., 2019). The CWT can be thought of as consecutive band-pass filters (Grinsted et al., 2004) wherein a mother wavelet, here, the Morlet wavelet, is convolved with a timeseries signal. The average wavelet

power spectra were min-max normalized to allow for direct comparison between each well, as done in Rust et al. (2019). The time-averaged wavelet coherence was used to determine the correlation, in time-frequency space, between groundwater levels and ENSO (via the ONI), as well as between ENSO and SPI. The significance ($\alpha = 0.05$) of wavelet power, and coherence, were tested via Monte Carlo simulations ($n = 100$), against a null hypothesis that the time series are being driven by a lag-1 autoregressive process (Torrence & Compo, 1998).

3. Results

3.1. Groundwater Clustering and Memory Metrics

Groundwater level responses cluster into one of two groups based on their hydrograph shape (Figure 2), reflected in their autocorrelation structure (Figure 3). Cluster 1 wells are interpreted to respond to recharge from local precipitation, which is predominantly rainfall within the Fraser Valley. The autocorrelation structure of this cluster oscillates with a periodicity of 365 days (Figure 3a). Some wells display a weak semi-annual signal (Figures 3b and eg., OW474, 440, 462, 406). The strongest semi-annual signal within cluster 1 is from OW474, which likely reflects a snowmelt contribution to recharge from the adjacent local mountains. The average decorrelation lag time for cluster 1 is about 80 days, but ranges from 65 to 97 days. The linear decay rate, averages -0.012 days^{-1} . The dampening of the sinusoidal oscillation of the ACF is represented by the exponential decay rate which can be converted to a half-life. The half-life for cluster 1 is about 954 days. That is, approximately every 3 years, the ACF oscillation amplitude is diminished by half. Overall, cluster 1 wells are a group of relatively high memory aquifers, including all bedrock and confined aquifers within the study area.

Cluster 2 wells not only exhibit a groundwater response that is driven by recharge from local rainfall but are also significantly influenced by the Fraser River due to strong hydraulic connectivity. Cluster 2 wells are located in low lying unconfined aquifers adjacent to the Fraser River (Figure 1), facilitating hydraulic connectivity, which is best observed during the summer freshet (Figure 2). The hydraulic gradient between the Fraser River and OW485 confirms the degree of connectivity (Figure S10 in Supporting Information S1). During the brief summer freshet, hydraulic gradients are reversed, whereby the Fraser River contributes to adjacent aquifers. For a brief period during the summer, remote up-catchment mountains in the Fraser River Basin provide recharge to aquifers in the Fraser Valley. During non-freshet periods, aquifers contribute baseflow to the Fraser River, with gradients reaching their maximum during January (Figure S10 in Supporting Information S1). The sole exception is OW349 which has no hydraulic connection to the Fraser River but mimics its snowmelt response during the summer from the adjacent mountains. While many cluster 1 wells are situated near mountains, snowmelt seems to have little effect on summer groundwater levels.

Cluster 2 wells exhibit an autocorrelation structure that is markedly different than that of cluster 1 wells (Figure 3a), showing twice the ACF oscillation with dual frequency response in annual and semi-annual periodicities (Figure 3b). The additive nature of precipitation seasonality and aquifer-stream interactions with the Fraser River causes this dual signal. The average decorrelation lag time for cluster 2 is about 51 days, but ranges from 40 to 56 days. This average is significantly less than cluster 1 by about 30 days. The linear decay rate at early lag times is about -0.018 days^{-1} . The half-life for cluster 2 is about 392 days, whereby, approximately every year, the ACF oscillation amplitude is diminished by half, damped much more rapidly than in cluster 1.

In determining appropriate groundwater level lead adjustments (see Section 2.6), the cross-correlation between precipitation with groundwater levels, and groundwater level rates-of-change, shed some insight into response times (Table S1 in Supporting Information S1). The average groundwater level-precipitation cross-correlation lag time for confined aquifers (in cluster 1) is 77 days, ranging from 50 to 110 days. Fractured and unconfined aquifers (in cluster 1) average 58 days, ranging from 2 to 132 days. Cluster 2 wells tend to average 14.3 days, ranging from 2 to 53 days.

3.2. Intra-Annual Variability in Deluge and Drought

The majority of ARs make landfall from October to January but are focused to October and November (Figure 4a), when they are the most intense and likely to result in extreme precipitation events (Figure S11 in Supporting Information S1). Expressed as an amount contributed, ARs make up on average more than half of all precipitation received in October (Figure 4b); Gershunov et al. (2017) reported that October to December AR contribution averaged around 50%. Generally, between September and January, ARs contribute around 40% of

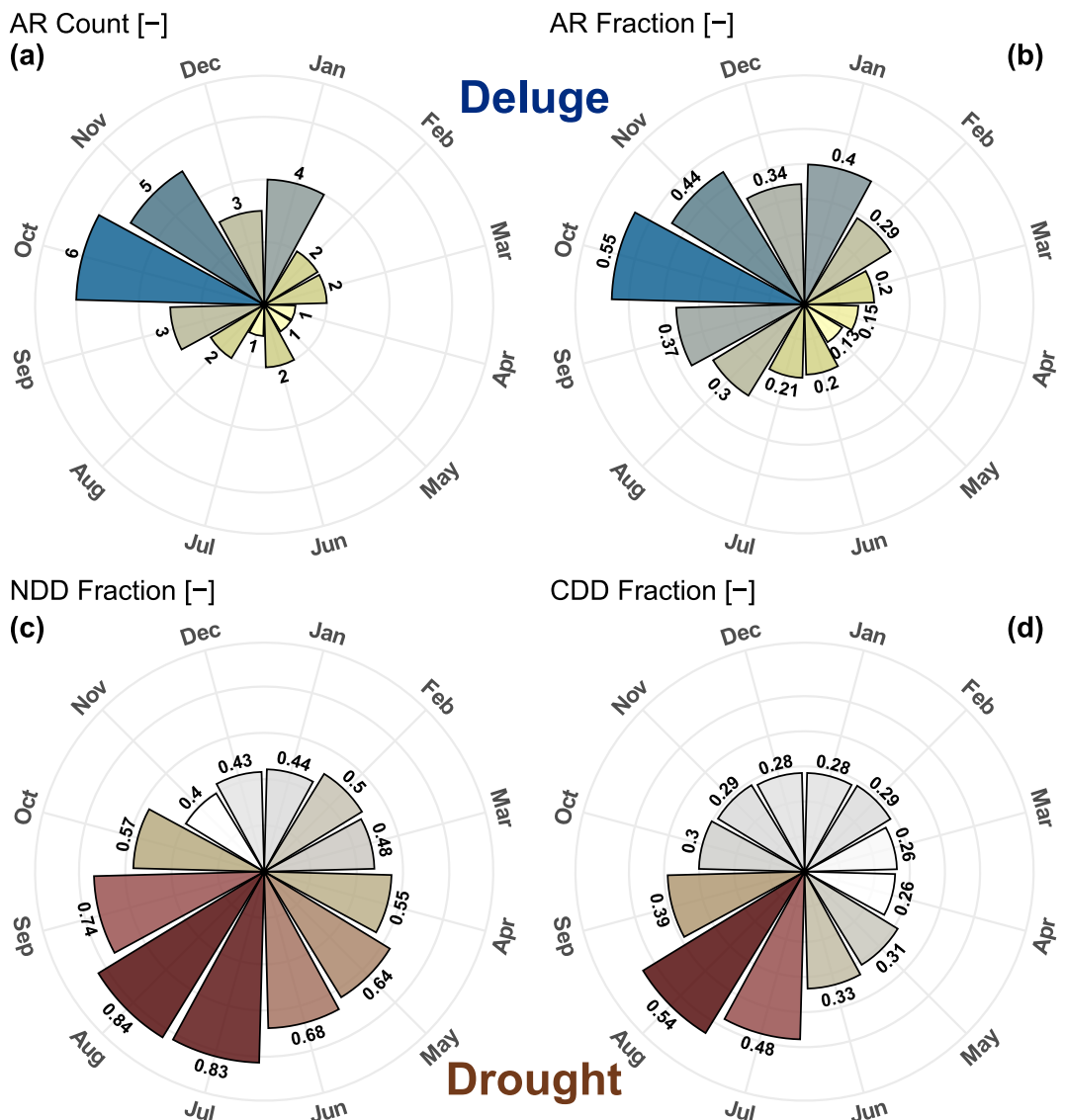


Figure 4. Deluge indicators as monthly averages of (a) atmospheric river (AR) counts and (b) AR fraction of precipitation. Drought indicators as (c) average number of dry days (NDD) and (d) consecutive dry days (CDD), as a fraction of total days in a month.

total precipitation. Atmospheric rivers are generally insignificant contributors to total, or extreme, precipitation during the spring to summer months (Figure 4b), as they are weaker in intensity and carry less moisture (Figure S11 in Supporting Information S1).

From April to October, on average, over 50% of the month receives no precipitation, and over 80% of days in August and July receive no precipitation (Figure 4c). Of those days in August and July, at least 2 weeks will be continuously dry (Figure 4d). Late summer to early autumn represents a significantly dry and drought-prone period. The transition between significantly dry and significantly wet is relatively rapid; August might be significantly dry but can transition to being significantly wet by October.

Monthly groundwater responses reveal a contrast between clusters and their relationship with intra-annual variability in wet and dry periods (Figure 5). Groundwater levels in cluster 1 wells increase as precipitation amounts increase, regardless of SPI (column 1—Figure 5a). Graphs for all wells are provided in Figure S12 in Supporting Information S1. During dry periods (brown) the slope of groundwater levels is steeper, when total precipitation is generally lower. This suggests that aquifers are more responsive to precipitation events during dry

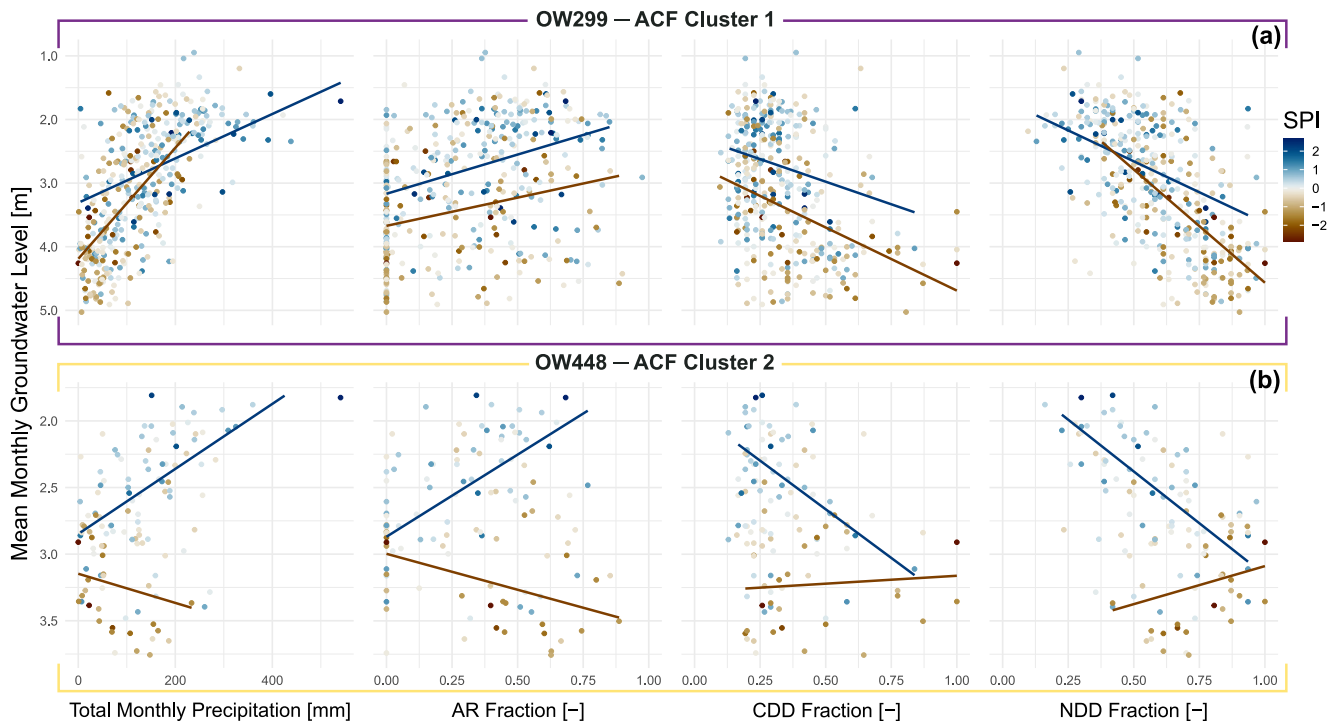


Figure 5. Mean monthly groundwater levels for (a) OW299 and (b) OW448 as a function of total monthly precipitation, monthly atmospheric river fraction, monthly CDD fraction, and monthly NDD fraction. Regression lines are included as visual guides.

periods compared to wet periods. Conversely, during wet periods, the groundwater level response slope is shallower, suggesting that more precipitation does not necessarily result in higher groundwater levels (column 1, Figure 5a). In this case, the infiltration capacity may be reached, resulting in more overland flow. For cluster 1 wells, as more precipitation is contributed by ARs (i.e., the AR fraction increases), groundwater levels increase regardless of wet or dry conditions (column 2, Figure 5a). Generally, groundwater level variability in response to higher AR fraction of precipitation is quite high (Figure S13 in Supporting Information S1).

Cluster 2 wells tend to show a diverging pattern whereby, during a dry period (negative SPI), the groundwater level slope is negative (column 1, Figure 5b). During a dry period, as precipitation amounts increase, groundwater levels seem to decrease. Cluster 2 wells also show a diverging pattern as the AR fraction of precipitation increases (column 2, Figure 5b). AR maximum event intensity follows a similar response; greater intensity ARs are associated with higher groundwater levels, except during dry periods (Figure S14 in Supporting Information S1). More intense events are likely to contribute a greater amount to the fraction of precipitation, leading to a greater recharge potential. Some cluster 1 wells (e.g., OW406 and OW450 in Figure S13 in Supporting Information S1) show a diverging pattern of lower groundwater levels with greater AR fractions of precipitation. This may reflect a weak influence from the Fraser River, given their distance to the river (Figure 1), but the local climate signal is stronger placing them in cluster 1. Overall, this dichotomy between cluster response stresses the adage of correlation versus causation. Greater precipitation does not cause lower groundwater levels. Rather, cluster 2 groundwater levels are higher in the summer than in early autumn, opposite to cluster 1. This shifts the summer groundwater level mean to be higher than the autumn mean (Figure 6), resulting in the diverging patterns observed in Figure 5b.

Longer dry spells (CDD) are associated with lower groundwater levels in both clusters, although cluster 2 wells show a flat response during negative SPI periods (column 3, Figure 5). CDD fractions less than around 0.5 (two weeks without precipitation) show considerable variations in groundwater level, regardless of dry or wet periods (Figure S15 in Supporting Information S1). A greater NDD is associated with lower groundwater levels (column 4, Figure 5a) regardless of SPI; but the dry period response from cluster 2 is opposite that of cluster 1 (column 4, Figure 5b), increasing during local climatological dry period of the Fraser Valley and Fraser River freshet.

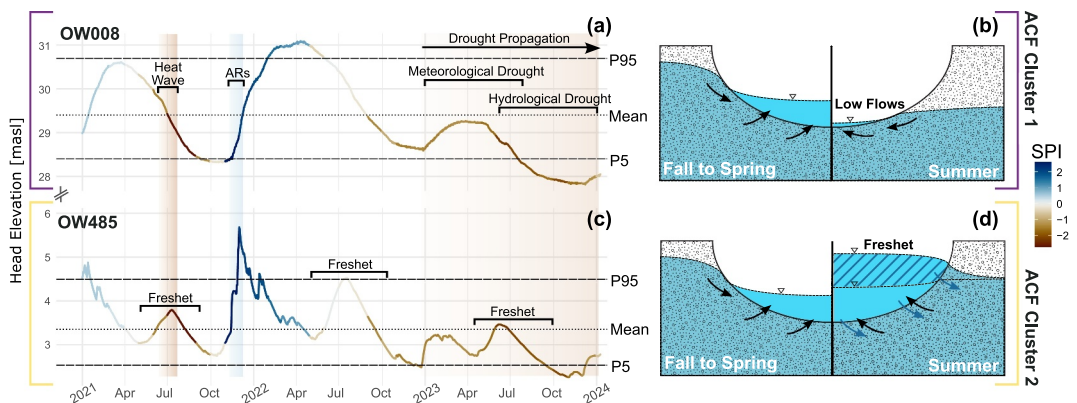


Figure 6. Daily timeseries for wells in each cluster illustrating extreme events on groundwater response (a) for OW008 and (c) OW485. Conceptual models for seasonal aquifer-stream interactions in panel (b) cluster 1 where groundwater primarily contributes to baseflow (black arrows), and in panel (d) cluster 2 where the Fraser River's freshet can reverse hydraulic gradients (striped), reversing flow and recharging aquifers (blue arrows).

Figure 6 offers a more intuitive visualization of the patterns observed in Figure 5, highlighting groundwater responses to extreme events experienced in recent years (2021–2023). The summer of 2021 saw a heatwave-intensified meteorological drought with considerably below normal summer precipitation (Figure 2a). By August 2021, cluster 2 maintained average levels while cluster 1 wells fell much below normal (Figures 6a and c), highlighting cluster 2's ability to delay the onset of drought propagation via recharge from the Fraser River (Figure 6d). A total of 541 mm of precipitation in November 2021 from ARs, of which 153 mm fell in only two days, promptly offset the summer deficit, substantially raising groundwater levels across the Fraser Valley (Figures 6a and c). Record low winter precipitation in 2023 (Figure 2a) resulted in rapid drought propagation in cluster 1 (Figure 6a), causing groundwater levels to remain well below normal into the autumn and winter. Cluster 2 aquifers were able to maintain around average groundwater levels in the summer, from freshet recharge; however, they eventually reached record lows (Figure 6c). Small streams connected to cluster 1 aquifers, which are also controlled by local climate, depend on groundwater baseflow to sustain summer flows (Figure 6b), resulting in many dry stream reaches across the Fraser Valley in 2023.

3.3. Inter-Annual Variability in Deluge and Drought

The Fraser Valley averages 34 ARs (range: 16–53) per year (1980–2022), contributing to over a third (AR fraction: 37%), or about 571 mm, of total annual precipitation (1,542 mm) (Figure 7 and Table S2 in Supporting Information S1). These results agree with regional AR studies that include the Pacific Northwest (Borkotoky et al., 2023; Collow et al., 2022; Gershunov et al., 2017; Tan et al., 2022). Typically, about 60% of the year receives no precipitation, leaving only 40% of the year for potential recharge. Every year averages nearly a full month that receives no precipitation, typically during late summer.

Figure 7b plots the last decade of groundwater levels for both OW299 (cluster 1) and OW448 (cluster 2), which have similar depths to water table and median groundwater levels. The interquartile range for OW299 is much wider than for OW448, displaying a greater variability in groundwater level throughout a given year. Low groundwater levels occur around September, while highs are reached around December (Figure 7b).

Aside from total precipitation, the most influential driver of intra-annual groundwater level variation seems to be the timing and distribution of precipitation events. For example, despite an above average snowpack in 2022, nearly three months (end-July to mid-October) without precipitation affected both clusters significantly, resulting in December groundwater levels well below the annual median (Figures 6 and 7b). Warmer winters result in substantially lower snowpacks in the Pacific Northwest, even if precipitation amounts are within a normal range, as evidenced in 2015 (Mote et al., 2016). Accordingly, cluster 2 wells show lower median groundwater levels in years with below average snowpack (Figure 7b). These results also support the importance of ARs as significant contributors to snowpack accumulation, as above average April 1st SWE in 2020 and 2021 were also years that experienced over 50 ARs (Figure 7a). Despite the second highest CDD run in over 40 years, 2021 groundwater

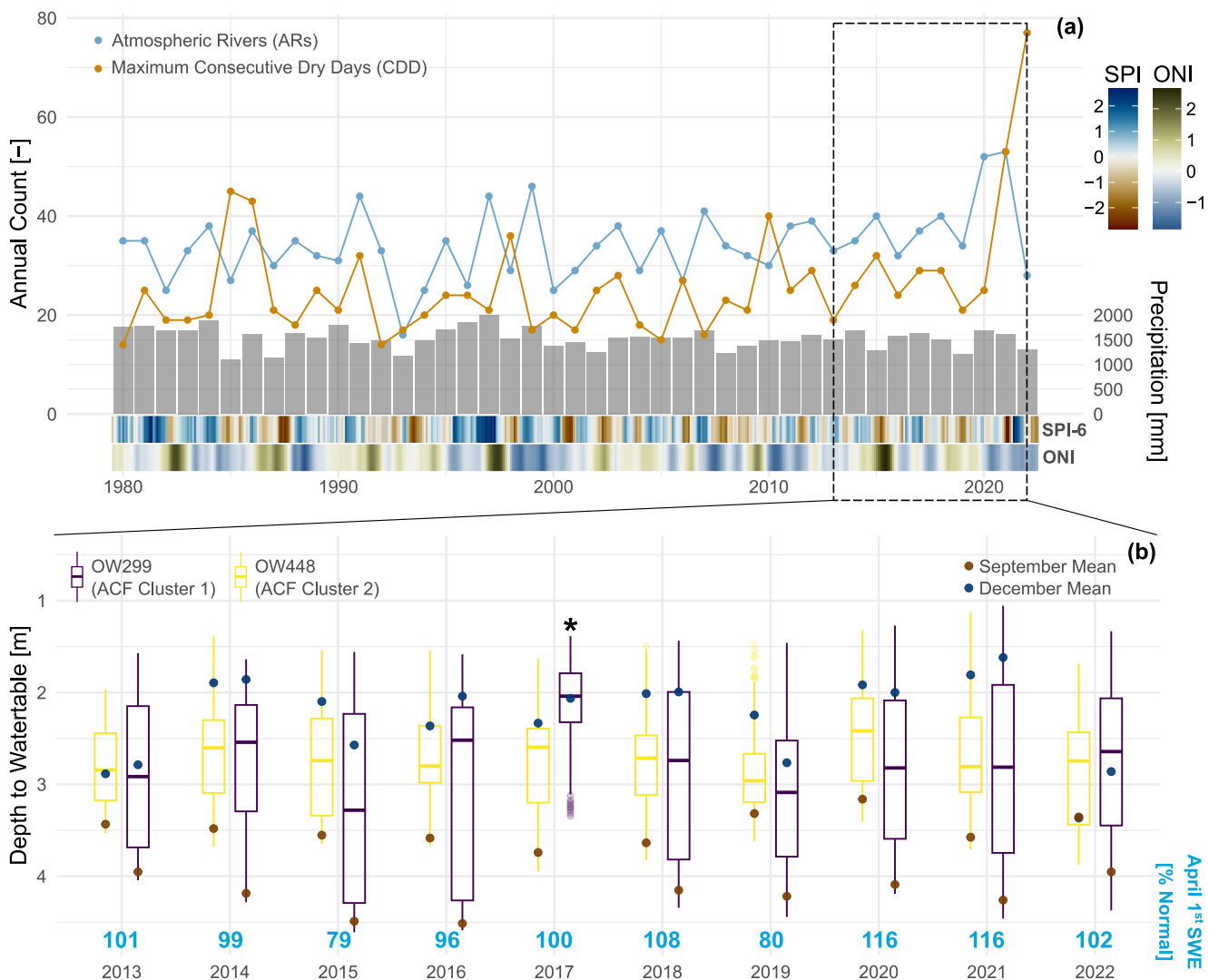


Figure 7. (a) Four decades of hydroclimatology (b) Latest decade of water table variations in both clusters as a response to precipitation, atmospheric rivers, and max CDDs. September (blue) and December (brown) monthly means typify average dry period lows and wet period highs, respectively. April 1st snow water equivalent (SWE) percentage of normal snowpack averaged across the entire Fraser River Basin is sourced from the BC Snow Survey and Water Supply Bulletin (available from <https://www2.gov.bc.ca/gov/content/environment/air-land-water/water/drought-flooding-dikes-dams/river-forecast-centre/snow-survey-water-supply-bulletin>). *The 2017 boxplot for OW299 is included for completeness despite missing data from August to November.

levels across the Fraser Valley were at record highs after receiving 56% of precipitation as ARs (Figure 6 and Table S2 in Supporting Information S1).

Based on wavelet analysis, the cyclicity in dry ($SPI < -1$) and wet ($SPI > 1$) periods tends to follow on average a 2-year cycle (Figure S17 in Supporting Information S1) with a dominant periodicity of 1–3 years. Cyclicalities in extremes tend to correlate more broadly with cycles of ENSO based on the wavelet coherence between SPI and ONI, although this is confined to select time periods (Figure S18 in Supporting Information S1). SPI and ONI show strong coherence in the 2-year periodicity from 1980 to 1990, 1- to 4-year periodicity from 1998 to 2002, and 3-year periodicity from 2015 to 2020 (Figure S18 in Supporting Information S1). This is broadly reflected in inter-annual groundwater level variations in the last decade (Figure 7b). Looking at the wavelet coherence between groundwater levels and ENSO cycles, there is significant coherence in the 1- and 2-to-7-year periodicities for cluster 1 wells (Figure S19 in Supporting Information S1). Consistent with the findings in Corona et al. (2018), the ENSO signal is preserved within the recharge signal for most aquifers. The variations in dry-wet periods with ENSO cycles highlights the inter- and intra-annual temporal complexities in climate and weather over the

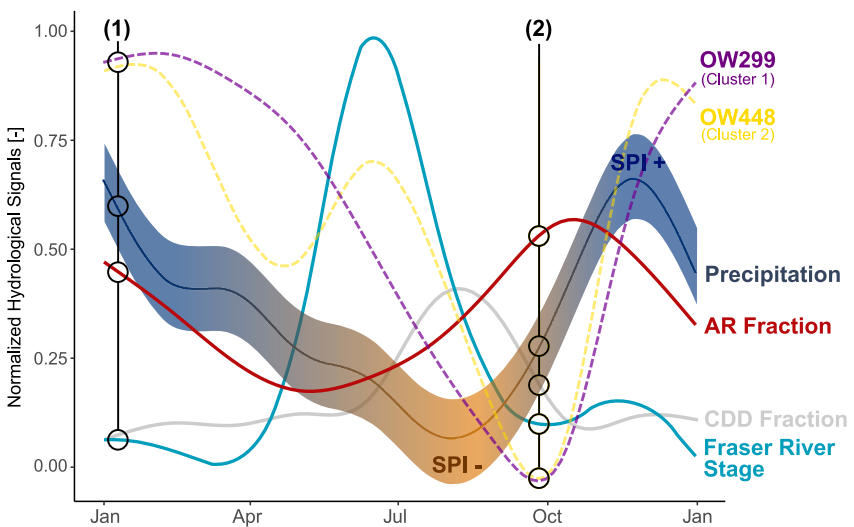


Figure 8. Integrated plot of normalized hydrological signals summarizing the controls of the Fraser River stage, AR fraction of precipitation, CDD fraction, and precipitation, on the groundwater level response in representative cluster 1 (observation wells (OW) 299) and cluster 2 (OW 448) wells. (a) Concurrent periods of high atmospheric river precipitation fractions and positive standardized precipitation index, associated with higher groundwater levels, present in both clusters. (b) Groundwater level minima driven by local climate, in both clusters.

decades: flash droughts can occur during wet winter La Niña (see 2021), while intense ARs can occur dry winter El Niño (see 2015).

4. Discussion

4.1. Groundwater Response to Extremes

Understanding groundwater responses to extremes is contingent on understanding the physical processes that underpin the hydrogeological context. For example, in the semi-arid tropics of East Africa, extreme rainfall is required to overcome evapotranspiration and provide diffuse recharge as well as focused recharge from ephemeral streamflow (Taylor et al., 2013). In contrast, in snowmelt-dominated mountainous regions, extreme rainfall during the winter can cause rain-on-snow events, leading to more overland flow and less recharge (Siirila-Woodburn et al., 2023). In this study, ARs are shown to be an important mechanism of recharge, but the dynamics of the Fraser River boundary condition influence the groundwater response to extremes in some aquifers, but not in others. Clustering was key in being able to systematically differentiate the aquifer responses to extremes. The superposition of signals in Fraser Valley aquifers are summarized in Figure 8. As illustrated in Figure 8, during winter (a), precipitation (positive SPI) and the fraction of ARs are both high, while the Fraser River stage (discharge) is low. Both wells (OW 299 representing a cluster 1 well and OW 448 representing a cluster 2 well) have high groundwater levels in response to recharge from autumn and winter precipitation and ARs.

The Fraser River, acting as a boundary condition, begins to exert a much stronger control as local precipitation starts to decline. Groundwater levels in Cluster 2 wells begin to recede, and have much lower groundwater levels than cluster 1 wells in the spring. During the summer, cluster 1 wells show a decrease in groundwater levels proportional to decreased precipitation and increased CDDs. Conversely, groundwater levels in cluster 2 well begin to rise, as their response is controlled more by the Fraser River boundary condition than local precipitation deficits. Both clusters reach minima in early autumn, around October, as precipitation and AR fraction increase. The Fraser River influence on cluster 2 wells is relatively brief, and by early autumn, these wells revert to responding to the availability of diffuse recharge from local precipitation, matching cluster 1.

Cluster 2 wells are more drought resilient (to local climate) over nearly the entirety of the summer, as also evidenced in Figure 6. The snowpack built up across the Fraser River Basin can sustain the Fraser River during local meteorological droughts (high fraction of NDD and CDD). However, a low snowpack (snow drought) or a rapid rise in spring temperatures across the basin generally results in lower summer cluster 2 groundwater levels,

as shown in the summer of 2023 (Figure 6c). Both clusters are particularly sensitive to the number of CDD, which is the main driver for summer and autumn groundwater declines.

4.2. Groundwater Memory Characteristics

As discussed by Duvert et al. (2015) and Sorensen et al. (2021), the process of clustering hydrographs and analyzing the autocorrelation structure reveals an abundance of information on physical processes as well as insight into the observed response to extremes. We found that while the ACF was an important technique for deriving groundwater memory characteristics, our results suggest broader implications for elucidating the influence of boundary conditions on groundwater response. We show that physical hydrogeological boundaries (aquifer-stream connectivity) can significantly influence the autocorrelation structure of groundwater levels.

As expected, the hydraulic properties of an aquifer do not fully explain the variance in ACF-derived memory metrics (Figure S21 in Supporting Information S1). To explain why, we focus on the decorrelation lag time and the damped decay rate half-life. The linear decay rate is log-correlated with decorrelation lag time and therefore is redundant (Figure S20 in Supporting Information S1). The decorrelation lag times for the porous aquifers ranged from 40 to 97 days, in good agreement with other groundwater studies across the globe. Schuler et al. (2022) reported decorrelation lag times between 45 and 154 days in porous aquifers across Ireland, whilst Duy et al. (2021) reported values from 35 to 199 days in porous aquifers across the Mekong Delta in Vietnam.

Estimating aquifer hydraulic properties is challenging and often highly uncertain (Kuang et al., 2020), yet is imperative in accurately characterizing groundwater memory. Hydraulic diffusivity acts to dampen hydraulic head responses (H. F. Wang, 2020), integrating transmissivity and storativity into a single property that represents the efficiency in signal propagation. We argue that diffusivity is a fundamental property in governing aquifer memory. High diffusivity aquifers have a more rapid groundwater level recession (Corona et al., 2023) with a less damped recharge signal (Corona et al., 2018), because the response can be propagated more efficiently through the vadose zone. Of the wells with hydraulic property data (26), diffusivity spans over five orders of magnitude ranging from 0.007 to 260.7 m²/s. Cluster 2 wells have the greatest diffusivity values with a geometric mean of 168.1 m²/s (range: 101.3–260.7 m²/s), while cluster 1 wells have a much greater range of diffusivity values with a geometric mean of 0.5 m²/s (range: 0.007–205.9 m²/s). Generally, a lower diffusivity is correlated with higher values of both memory metrics. This relationship is stronger ($R^2 = 0.51$) when considering diffusivity as a function of decorrelation lag time (Figure S21a in Supporting Information S1). While the damped decay rate half-life tends to decrease with decreasing diffusivity, the relationship is weaker ($R^2 = 0.25$) (Figure S21b in Supporting Information S1). As more than half of the total variation in decorrelation lag time is explained by diffusivity, this suggests that the damped decay rate half-life reflects a more complex set of factors influencing the ACF.

The disparity in cluster memory metrics raises an important question: do cluster 2 wells really have lower memory than cluster 1 wells? Or would both clusters have similar memory metrics had the Fraser River been absent? We can tease out the answer by observing the relationship between the linear decay rate and the distance of the well to the Fraser River (Figure S21 in Supporting Information S1). Cluster 2 wells do tend to be more diffusive by nature of their location and fluvial depositional environment. However, their linear decay rate increases logarithmically with increasing distance away from the Fraser River, approaching cluster 1 decay rates (Figure S22 in Supporting Information S1). The linear decay rate for cluster 1 wells seems independent of distance to the Fraser River, despite also including aquifers that are relatively highly diffusive. We posit that cluster 2 wells have lower memory metrics, in part due to higher diffusivity, but also because of how effective the Fraser River is at behaving as a boundary condition to groundwater in these aquifers. This further supports the idea that groundwater memory is controlled not only by physical catchment characteristics, but also by the superposition of signals from different physical processes.

4.3. Implications for Groundwater Management

Nearly all Fraser Valley aquifers support agricultural activity, primarily used for irrigation. Peak water use in the South Coast generally occurs from June to September, concomitant with low precipitation. At an hourly recording rate, none of the wells used in this analysis, aside from OW441, showed sub-daily to daily pumping signals. However, there are likely seasonal declines in groundwater level at some scale that are related to pumping associated with irrigation. These pumping signals are not strong enough to overwrite the recharge signal or Fraser

River signal, meaning that the clustering results are valid. Nevertheless, we acknowledge that the memory metrics may be different had there not been any pumping signal.

We suggest that cluster 1 wells should be at a higher priority for drought monitoring, as these aquifers respond only to local climate. Groundwater abstraction in cluster 2 wells could be focused during the Fraser River freshet, typically May to June, and minimized closer to the Fraser River autumn minima, usually between September and October (Figure 8).

During the autumn and winter when ARs can lead to rapid rises in the water table, groundwater flooding is a significant risk. The November 2021 ARs caused catastrophic widespread surface water flooding (Figure 6), especially in the area of the old Sumas Lake underlain by poorly drained sediments (Figure 1). Unsurprisingly, as cluster 2 associated-aquifers coincide with the Fraser River floodplain, they have been mapped as high flood risk potential (Fraser Basin Council, 2023). Moreover, these floodplain soils are host to highly productive agricultural fields that rely on groundwater for irrigation. Irrigation bypass flow, wherein groundwater abstracted from confined aquifers is routed to unconfined aquifers via irrigation, poses an increased flood risk (Houspanossian et al., 2023). Focusing abstraction during the freshet peak while storing this water for irrigation during the Fraser River recession might mitigate this risk, as opposed to continuous pumping until the autumn rains. Extreme precipitation events in North America, have, and will continue to increase in frequency (Du et al., 2022) and intensity (Li et al., 2019; Prein et al., 2017; Sun et al., 2021). Specifically, ARs at midlatitudes are projected to become stronger and more frequent (Espinoza et al., 2018; S. Wang et al., 2023), especially in the Pacific Northwest (Gershunov et al., 2019; O'Brien et al., 2022), resulting in less snowfall and more rainfall at mid-elevations (Payne et al., 2020). Presumably, groundwater flooding across the Fraser Valley is likely to become more frequent, especially during late autumn.

The Fraser River Basin has been shifting from a snow-dominated regime to a hybrid nival-pluvial regime over the past decades (Kang et al., 2014), with future climate warming projected to lead to decreased and earlier peak summer melt (Islam et al., 2019). Climate warming has already begun to affect snow droughts and winter snowpack accumulation across the Pacific Northwest (Mote et al., 2016). Islam et al. (2017) show that the fraction of precipitation falling as snow across the basin is projected to significantly decrease, up to 50% by 2050, in addition to an earlier freshet. Although autumn streamflow extremes might be more likely with the projected increase in landfalling ARs across the basin (Curry et al., 2019).

AR-laden moisture can continue to be transported inland, all the way to central and eastern Canada causing additional rainfall events within 12 days of making landfall on the coast (Vallejo-Bernal et al., 2023). Within a single day of making landfall on the coast, these ARs can contribute significantly to snowpack accumulation in the Rocky Mountains, the headwaters of the Fraser River, even recharging groundwater (Figure S23 in Supporting Information S1). However, warming AR circulations have contributed to an overall decrease in AR-related snowfall, even at higher elevations (Sharma & Déry, 2020), which has the potential to contribute further to an already shifting Fraser River Basin regime.

5. Conclusions

Extreme events, in both the occurrence and magnitude of ARs and droughts, will continue to increase under a warming climate, shifting groundwater behavior across the Pacific Northwest. We analyzed groundwater levels across the Fraser Valley in the South Coast of BC with the objective of determining groundwater responses to ARs and drought. On average, 34 ARs make landfall in the Fraser Valley every year, contributing to, on average, 37% of annual precipitation. During peak winter recharge (October to January), around 40% of total precipitation is contributed by ARs, concentrated to October and November. During drought-prone periods (April–September), more than 50% of days receive no precipitation, with typically 26 consecutive dry days. Annual average precipitation, 1,542 mm, is concentrated to only about 40% of the year, indicating a concentrated recharge period.

By examining the autocorrelation structure of groundwater levels, a common approach to characterizing aquifer memory, we demonstrated that aquifers in the South Coast region of BC can be influenced by both local and non-local drivers of recharge, mediated by the hydraulic connectivity to the Fraser River. Two distinct clusters are identified using autocorrelation characteristics. Cluster 1 wells respond to recharge from local precipitation and are quick to respond both ARs during winter recharge season and significant rainfall deficits during the summer. Predictably, cluster 1 groundwater levels increase as the total amount of precipitation or the fraction of AR

precipitation increases, regardless of wet or dry season. Similarly, cluster 1 wells respond predictably to dry conditions, with groundwater levels declining with longer dry spells. Cluster 2 wells also respond to recharge from local precipitation during the winter, but are substantially influenced by the Fraser River, which acts as a hydraulic boundary. This hydraulic connectivity between cluster 2 wells and the Fraser River leads to a shift in the timing of groundwater hydrographs relative to local climate conditions. Summer groundwater drought is mediated by the Fraser River's summer freshet, by shifting the recession in cluster 2 wells.

Despite experiencing the same climate, the differentiation in the dominant recharge mechanism and superposition of processes (local recharge and hydraulic boundary conditions) ultimately controls the groundwater response to extremes. Therefore, in this hydrological setting, groundwater memory is controlled by the intrinsic hydraulic properties of an aquifer and encodes the effects of hydraulic boundary conditions. The identification of different drivers of groundwater response can aid in more effective groundwater management strategies in dealing with the effects of climate change, as the hydrological regime of the Fraser River Basin and similar basins across the Pacific Northwest shift from being snow-to rain-dominated.

Conflict of Interest

The authors declare no conflicts of interest relevant to this study.

Data Availability Statement

The AR catalogue (Rutz et al., 2014 method), used to derive the AR catalogue for the Fraser Valley, is available through <https://www.earthsystemgrid.org/dataset/ucar.cgd.artmip.tier1.catalogues.rutz.html>. The derived Fraser Valley AR catalogue, well and aquifer information including memory metrics (Table S1 in Supporting Information S1), PGOWN observation well data, and code used in the analysis, are available in repository hosted on Hydroshare (Nott et al., 2024). Open data from the government of British Columbia for provincial groundwater observation well data and aquifer information are available from <https://catalogue.data.gov.bc.ca/dataset/57c55f10-cf8e-40bb-aae0-2eff311f1685> and <https://catalogue.data.gov.bc.ca/dataset/099d69c5-1401-484d-9e19-c121ccb7977c>, respectively. Meteorological data for BC are available at <https://services.pacificclimate.org/met-data-portal-pcds/app/>. Hydrometric data are available at https://wateroffice.ec.gc.ca/search/real_time_e.html.

Acknowledgments

We thank Brian Kawzenuk from the Center for Western Weather and Water Extremes (CW3E) for help accessing the AR catalogue. We also thank the three anonymous reviewers for their suggestions for improving this paper. This project was funded by the Pacific Institute for Climate Solutions (PICS) as a PICS Opportunity Project and by a Discovery Grant to D. Allen from the Natural Sciences and Engineering Research Council of Canada.

References

- Abarca, E., Karam, H., Hemond, H. F., & Harvey, C. F. (2013). Transient groundwater dynamics in a coastal aquifer: The effects of tides, the lunar cycle, and the beach profile. *Water Resources Research*, 49(5), 2473–2488. <https://doi.org/10.1002/wrcr.20075>
- AghaKouchak, A., Mirchi, A., Madani, K., Baldassarre, G. D., Nazemi, A., Alborzi, A., et al. (2021). Anthropogenic drought: Definition, challenges, and opportunities. *Reviews of Geophysics*, 59(2), e2019RG000683. <https://doi.org/10.1029/2019RG000683>
- Armstrong, J. E. (1981). *Post-Vashon Wisconsin glaciation, Fraser lowland, British Columbia (Bulletin 322)*. Geological Survey of Canada. <https://doi.org/10.4095/10952>
- Armstrong, J. E. (1984). *Environmental and engineering applications of the surficial geology of the Fraser lowland* (pp. 83–23). Geological Survey of Canada. <https://doi.org/10.4095/119727>
- Ataei-Ashtiani, B., Volker, R. E., & Lockington, D. A. (2001). Tidal effects on groundwater dynamics in unconfined aquifers. *Hydrological Processes*, 15(4), 655–669. <https://doi.org/10.1002/hyp.183>
- Barberio, M. D., Gori, F., Barbieri, M., Billi, A., Caracausi, A., De Luca, G., et al. (2020). New observations in Central Italy of groundwater responses to the worldwide seismicity. *Scientific Reports*, 10(1), 17850. <https://doi.org/10.1038/s41598-020-74991-0>
- Barker, L. J., Hannaford, J., Chiverton, A., & Svensson, C. (2016). From meteorological to hydrological drought using standardised indicators. *Hydrology and Earth System Sciences*, 20(6), 2483–2505. <https://doi.org/10.5194/hess-20-2483-2016>
- Barlow, P. M., & Leake, S. A. (2012). *Streamflow depletion by wells—understanding and managing the effects of groundwater pumping on streamflow (circular 1376)*. U.S. Geological Survey. Retrieved from <http://pubs.usgs.gov/circ/1376/>
- Bartusek, S., Kornhuber, K., & Ting, M. (2022). 2021 North American heatwave amplified by climate change-driven nonlinear interactions. *Nature Climate Change*, 12(12), 1143–1150. <https://doi.org/10.1038/s41558-022-01520-4>
- BCGS. (2019). *Bedrock geology*. BC Geological Survey. Retrieved from <https://catalogue.data.gov.bc.ca/dataset/ef8476ed-b02d-4f5c-b778-0d44c9126144>
- Beck, H. E., Zimmermann, N. E., McVicar, T. R., Vergopolan, N., Berg, A., & Wood, E. F. (2018). Present and future Köppen-Geiger climate classification maps at 1-km resolution. *Scientific Data*, 5(1), 180214. <https://doi.org/10.1038/sdata.2018.214>
- Bergbuijs, W. R., Luijendijk, E., Moeck, C., van der Velde, Y., & Allen, S. T. (2022). Global recharge data set indicates strengthened groundwater connection to surface fluxes. *Geophysical Research Letters*, 49(23), e2022GL099010. <https://doi.org/10.1029/2022GL099010>
- Bergbuijs, W. R., & Slater, L. J. (2023). Groundwater shapes North American river floods. *Environmental Research Letters*, 18(3), 034043. <https://doi.org/10.1088/1748-9326/acbecc>
- Bierkens, M. F. P., & Wada, Y. (2019). Non-Renewable groundwater use and groundwater depletion: A review. *Environmental Research Letters*, 14(6), 063002. <https://doi.org/10.1088/1748-9326/ab1a5f>

- Bloomfield, J. P., & Marchant, B. P. (2013). Analysis of groundwater drought building on the standardised precipitation index approach. *Hydrology and Earth System Sciences*, 17(12), 4769–4787. <https://doi.org/10.5194/hess-17-4769-2013>
- Borkotoky, S. S., Williams, A. P., & Steinschneider, S. (2023). Six hundred years of reconstructed atmospheric river activity along the US West Coast. *Journal of Geophysical Research: Atmospheres*, 128(12), e2022JD038321. <https://doi.org/10.1029/2022JD038321>
- Brigode, P., Mićović, Z., Bernardara, P., Paquet, E., Garavaglia, F., Gailhard, J., & Ribstein, P. (2013). Linking ENSO and heavy rainfall events over coastal British Columbia through a weather pattern classification. *Hydrology and Earth System Sciences*, 17(4), 1455–1473. <https://doi.org/10.5194/hess-17-1455-2013>
- Bronaugh, D., Schoeneberg, A., & Zeman, L. (2023). Zyp (0.11-1) [Computer Software]. <https://cran.r-project.org/web/packages/zyp/index.html>
- Brooks, P. D., Gelderloos, A., Wolf, M. A., Jamison, L. R., Strong, C., Solomon, D. K., et al. (2021). Groundwater-mediated memory of past climate controls water yield in snowmelt-dominated catchments. *Water Resources Research*, 57(10), e2021WR030605. <https://doi.org/10.1029/2021WR030605>
- Brunner, M. I. (2023). Floods and droughts: A multivariate perspective. *Hydrology and Earth System Sciences*, 27(13), 2479–2497. <https://doi.org/10.5194/hess-27-2479-2023>
- Carmichael, V. (2013). *Compendium of Re-evaluated pumping tests in the regional district of nanaimo, BC* (p. 941). Ministry of Environment. Retrieved from https://a100.gov.bc.ca/pub/acat/documents/r36013/RDNPumpingTestReport-Final_1364940347722_26e407c53d6a979b00218722372c4fb2ea7d6c7c60110e4f661734c7bde1889c.pdf
- Charrad, M., Ghazzali, N., Boiteau, V., & Niknafs, A. (2014). NbClust: An R package for determining the relevant number of clusters in a data set. *Journal of Statistical Software*, 61(6), 1–36. <https://doi.org/10.18637/jss.v061.i06>
- Chen, X., Leung, L. R., Wigmosta, M., & Richmond, M. (2019). Impact of atmospheric rivers on surface hydrological processes in Western U.S. Watersheds. *Journal of Geophysical Research: Atmospheres*, 124(16), 8896–8916. <https://doi.org/10.1029/2019JD030468>
- Clague, J. J. (1994). *Quaternary stratigraphy and history of south-coastal British Columbia*. Natural Resources Canada. 481. <https://doi.org/10.4095/203249>
- Clague, J. J., & James, T. S. (2002). History and isostatic effects of the last ice sheet in southern British Columbia. *Quaternary Science Reviews*, 21(1), 71–87. [https://doi.org/10.1016/S0277-3791\(01\)00070-1](https://doi.org/10.1016/S0277-3791(01)00070-1)
- Clague, J. J., Luternauer, J. L., & Hebda, R. J. (1983). Sedimentary environments and postglacial history of the Fraser Delta and lower Fraser Valley, British Columbia. *Canadian Journal of Earth Sciences*, 20(8), 1314–1326. <https://doi.org/10.1139/e83-116>
- Clague, J. J., & Ward, B. (2011). Chapter 44—Pleistocene glaciation of British Columbia. In J. Ehlers, P. L. Gibbard, & P. D. Hughes (Eds.), *Developments in quaternary sciences* (Vol. 15, pp. 563–573). Elsevier. <https://doi.org/10.1016/B978-0-444-53447-7.00044-1>
- Collow, A. B. M., Mersiovsky, H., & Bosilovich, M. G. (2020). Large-scale influences on atmospheric river-induced extreme precipitation events along the coast of Washington State. *Journal of Hydrometeorology*, 21(9), 2139–2156. <https://doi.org/10.1175/JHM-D-19-0272.1>
- Collow, A. B. M., Shields, C. A., Guan, B., Kim, S., Lora, J. M., McClenny, E. E., et al. (2022). An overview of ARTMIP's tier 2 reanalysis intercomparison: Uncertainty in the detection of atmospheric rivers and their associated precipitation. *Journal of Geophysical Research: Atmospheres*, 127(8), e2021JD036155. <https://doi.org/10.1029/2021JD036155>
- Condon, L. E., & Maxwell, R. M. (2019). Simulating the sensitivity of evapotranspiration and streamflow to large-scale groundwater depletion. *Science Advances*, 5(6), eaav4574. <https://doi.org/10.1126/sciadv.aav4574>
- Corona, C. R., & Ge, S. (2022). Examining subsurface response to an extreme precipitation event using HYDRUS-1D. *Vadose Zone Journal*, 21(3), e20189. <https://doi.org/10.1002/vzj2.20189>
- Corona, C. R., Ge, S., & Anderson, S. P. (2023). Water-table response to extreme precipitation events. *Journal of Hydrology*, 618, 129140. <https://doi.org/10.1016/j.jhydrol.2023.129140>
- Corona, C. R., Gurdak, J. J., Dickinson, J. E., Ferré, T. P. A., & Maurer, E. P. (2018). Climate variability and vadose zone controls on damping of transient recharge. *Journal of Hydrology*, 561, 1094–1104. <https://doi.org/10.1016/j.jhydrol.2017.08.028>
- Cox, S. E., & Kahle, S. C. (1999). Hydrogeology, ground-water quality, and sources of nitrate in lowland glacial aquifers of Whatcom County, Washington, and British Columbia, Canada. In *Water-resources investigations report* (pp. 98–4195). U.S. Geological Survey. <https://doi.org/10.3133/wri984195>
- Curry, C. L., Islam, S. U., Zwiers, F. W., & Déry, S. J. (2019). Atmospheric rivers increase future flood risk in western Canada's largest Pacific river. *Geophysical Research Letters*, 46(3), 1651–1661. <https://doi.org/10.1029/2018GL080720>
- Curry, C. L., & Zwiers, F. W. (2018). Examining controls on peak annual streamflow and floods in the Fraser River Basin of British Columbia. *Hydrology and Earth System Sciences*, 22(4), 2285–2309. <https://doi.org/10.5194/hess-22-2285-2018>
- CW3E. (2022). Distribution of landfalling atmospheric rivers over the U.S. West coast during water year 2022: Summary through march – center for western weather and water extremes. Retrieved from <https://cw3e.ucsd.edu/distribution-of-landfalling-atmospheric-rivers-over-the-u-s-west-coast-during-water-year-2022-summary-through-march/>
- Delbart, C., Valdés, D., Barbecot, F., Tognelli, A., & Couchoux, L. (2016). Spatial organization of the impulse response in a karst aquifer. *Journal of Hydrology*, 537, 18–26. <https://doi.org/10.1016/j.jhydrol.2016.03.029>
- Déry, S. J., Hernández-Henríquez, M. A., Owens, P. N., Parkes, M. W., & Petticrew, E. L. (2012). A century of hydrological variability and trends in the Fraser River Basin. *Environmental Research Letters*, 7(2), 024019. <https://doi.org/10.1088/1748-9326/7/2/024019>
- de Vries, J. J., & Simmers, I. (2002). Groundwater recharge: An overview of processes and challenges. *Hydrogeology Journal*, 10(1), 5–17. <https://doi.org/10.1007/s10040-001-0171-7>
- Dierauer, J. R., Whitfield, P. H., & Allen, D. M. (2018). Climate controls on runoff and low flows in mountain catchments of western North America. *Water Resources Research*, 54(10), 7495–7510. <https://doi.org/10.1029/2018WR023087>
- Du, H., Donat, M. G., Zong, S., Alexander, L. V., Manzanas, R., Kruger, A., et al. (2022). Extreme precipitation on consecutive days occurs more often in a warming climate. *Bulletin of the American Meteorological Society*, 103(4), E1130–E1145. <https://doi.org/10.1175/BAMS-D-21-0140.1>
- Duvert, C., Jourde, H., Raiber, M., & Cox, M. E. (2015). Correlation and spectral analyses to assess the response of a shallow aquifer to low and high frequency rainfall fluctuations. *Journal of Hydrology*, 527, 894–907. <https://doi.org/10.1016/j.jhydrol.2015.05.054>
- Duy, N. L., Nguyen, T. V. K., Nguyen, D. V., Tran, A. T., Nguyen, H. T., Heidbüchel, I., et al. (2021). Groundwater dynamics in the Vietnamese Mekong Delta: Trends, memory effects, and response times. *Journal of Hydrology: Regional Studies*, 33, 100746. <https://doi.org/10.1016/j.ejrh.2020.100746>
- ECCC. (2023). *Abbotsford airport climate station (ID 1100030/1100031)—environment and climate change Canada (ECCC)*. PCIC Data Explorer. Retrieved from <https://services.pacificclimate.org/met-data-portal-pcds/app/>
- ECCS. (2023). Provincial groundwater observation well network (PGOWN)—Ministry of environment and climate change strategy (ECCS)—groundwater levels. Retrieved from <https://catalogue.data.gov.bc.ca/dataset/57c55f10-cf8e-40bb-aae0-2eff311f1685>

- Eldardiry, H., Mahmood, A., Chen, X., Hossain, F., Nijssen, B., & Lettenmaier, D. P. (2019). Atmospheric river-induced precipitation and snowpack during the western United States cold season. *Journal of Hydrometeorology*, 20(4), 613–630. <https://doi.org/10.1175/JHM-D-18-0228.1>
- Espinoza, V., Waliser, D. E., Guan, B., Lavers, D. A., & Ralph, F. M. (2018). Global analysis of climate change projection effects on atmospheric rivers. *Geophysical Research Letters*, 45(9), 4299–4308. <https://doi.org/10.1029/2017GL076968>
- Fetter, C. W., & Kreamer, D. (2021). *Applied hydrogeology* (5th ed.). Waveland Press.
- Fleming, S. W., & Whitfield, P. H. (2010). Spatiotemporal mapping of ENSO and PDO surface meteorological signals in British Columbia, Yukon, and southeast Alaska. *Atmosphere-Ocean*, 48(2), 122–131. <https://doi.org/10.3137/AO1107.2010>
- Fraser Basin Council. (2023). Lower mainland flood management strategy—synthesis of technical analysis. Retrieved from https://www.fraserbasin.bc.ca/_Library/Water_Flood_Strategy/LMFMS_Synthesis_of_Technical_Analysis_Summer_2023_web.pdf
- Gelaro, R., McCarty, W., Suárez, M. J., Todling, R., Molod, A., Takacs, L., et al. (2017). The modern-era retrospective analysis for research and applications, version 2 (MERRA-2). *Journal of Climate*, 30(14), 5419–5454. <https://doi.org/10.1175/JCLI-D-16-0758.1>
- Gershunov, A., Shulgina, T., Clemesha, R. E. S., Guirguis, K., Pierce, D. W., Dettinger, M. D., et al. (2019). Precipitation regime change in Western North America: The role of atmospheric rivers. *Scientific Reports*, 9(1), 9944. <https://doi.org/10.1038/s41598-019-46169-w>
- Gershunov, A., Shulgina, T., Ralph, F. M., Lavers, D. A., & Rutz, J. J. (2017). Assessing the climate-scale variability of atmospheric rivers affecting western North America. *Geophysical Research Letters*, 44(15), 7900–7908. <https://doi.org/10.1002/2017GL074175>
- Gibbons, T. D., & Culhane, T. (1994). *Whatcom county hydraulic continuity investigation part 2: Basin study of johnson creek (OFTR 94-01)*. Washington State Department of Ecology. Retrieved from <https://www.whatcomcounty.us/DocumentCenter/View/4757/Exhibit-6-PDF?bidId=>
- Giese, M., Haaf, E., Heudorfer, B., & Barthel, R. (2020). Comparative hydrogeology – Reference analysis of groundwater dynamics from neighbouring observation wells. *Hydrological Sciences Journal*, 65(10), 1685–1706. <https://doi.org/10.1080/02626667.2020.1762888>
- Gleeson, T., Wang-Erlandsson, L., Porkka, M., Zipper, S. C., Jaramillo, F., Gerten, D., et al. (2020). Illuminating water cycle modifications and Earth system resilience in the Anthropocene. *Water Resources Research*, 56(4), e2019WR024957. <https://doi.org/10.1029/2019WR024957>
- Goldenson, N., Leung, L. R., Bitz, C. M., & Blanchard-Wrigglesworth, E. (2018). Influence of atmospheric rivers on mountain snowpack in the western United States. *Journal of Climate*, 31(24), 9921–9940. <https://doi.org/10.1175/JCLI-D-18-0268.1>
- Golder Associates Ltd. (2005). Comprehensive groundwater modelling assignment: Township of langley. Retrieved from <https://a100.gov.bc.ca/pub/acat/public/viewReport.do?reportId=57709>
- Grinsted, A., Moore, J. C., & Jevrejeva, S. (2004). Application of the cross wavelet transform and wavelet coherence to geophysical time series. *Nonlinear Processes in Geophysics*, 11(5/6), 561–566. <https://doi.org/10.5194/npg-11-561-2004>
- Gu, X., Sun, H., Zhang, Y., Zhang, S., & Lu, C. (2022). Partial wavelet coherence to evaluate scale-dependent relationships between precipitation/surface water and groundwater levels in a groundwater system. *Water Resources Management*, 36(7), 2509–2522. <https://doi.org/10.1007/s11269-022-03157-6>
- Guan, B., Waliser, D. E., Ralph, F. M., Fetter, E. J., & Neiman, P. J. (2016). Hydrometeorological characteristics of rain-on-snow events associated with atmospheric rivers. *Geophysical Research Letters*, 43(6), 2964–2973. <https://doi.org/10.1002/2016GL067978>
- Gudmundsson, L., & Stagge, J. H. (2016). SCI: Standardized climate indices such as SPI, SRI or SPEI. R package version [Computer Software], 1.0–2. <https://cran.r-project.org/web/packages/SCI/index.html>
- Gullacher, A., Allen, D. M., & Goetz, J. D. (2023). Early warning indicators of groundwater drought in mountainous regions. *Water Resources Research*, 59(8), e2022WR033399. <https://doi.org/10.1029/2022WR033399>
- Haaf, E., & Barthel, R. (2018). An inter-comparison of similarity-based methods for organisation and classification of groundwater hydrographs. *Journal of Hydrology*, 559, 222–237. <https://doi.org/10.1016/j.jhydrol.2018.02.035>
- Hellwig, J., de Graaf, I. E. M., Weiler, M., & Stahl, K. (2020). Large-scale assessment of delayed groundwater responses to drought. *Water Resources Research*, 56(2), e2019WR025441. <https://doi.org/10.1029/2019WR025441>
- Houspanessian, J., Giménez, R., Whitworth-Hulse, J. I., Nosetto, M. D., Tych, W., Atkinson, P. M., et al. (2023). Agricultural expansion raises groundwater and increases flooding in the South American plains. *Science*, 380(6652), 1344–1348. <https://doi.org/10.1126/science.add5462>
- Hu, Z., Zhou, Q., Chen, X., Li, J., Li, Q., Chen, D., et al. (2018). Evaluation of three global gridded precipitation data sets in central Asia based on rain gauge observations. *International Journal of Climatology*, 38(9), 3475–3493. <https://doi.org/10.1002/joc.5510>
- Iglesias, V., Travis, W. R., & Balch, J. K. (2022). Recent droughts in the United States are among the fastest-developing of the last seven decades. *Weather and Climate Extremes*, 37, 100491. <https://doi.org/10.1016/j.wace.2022.100491>
- Imagawa, C., Takeuchi, J., Kawachi, T., Chono, S., & Ishida, K. (2013). Statistical analyses and modeling approaches to hydrodynamic characteristics in alluvial aquifer. *Hydrological Processes*, 27(26), 4017–4027. <https://doi.org/10.1002/hyp.9538>
- Islam, S. U., Curry, C. L., Déry, S. J., & Zwiers, F. W. (2019). Quantifying projected changes in runoff variability and flow regimes of the Fraser River Basin, British Columbia. *Hydrology and Earth System Sciences*, 23(2), 811–828. <https://doi.org/10.5194/hess-23-811-2019>
- Islam, S. U., Déry, S. J., & Werner, A. T. (2017). Future climate change impacts on snow and water resources of the Fraser River Basin, British Columbia. *Journal of Hydrometeorology*, 18(2), 473–496. <https://doi.org/10.1175/JHM-D-16-0012.1>
- Jukić, D., & Denić-Jukić, V. (2004). A frequency domain approach to groundwater recharge estimation in karst. *Journal of Hydrology*, 289(1), 95–110. <https://doi.org/10.1016/j.jhydrol.2003.11.005>
- Kang, D. H., Shi, X., Gao, H., & Déry, S. J. (2014). On the changing contribution of snow to the hydrology of the Fraser River Basin, Canada. *Journal of Hydrometeorology*, 15(4), 1344–1365. <https://doi.org/10.1175/JHM-D-13-0120.1>
- Kassambara, A., & Mundt, F. (2020). factoextra: Extract and visualize the results of multivariate data analyses (R package version 1.0.7) [Computer software]. <https://CRAN.R-project.org/package=factoextra>
- King, A. D., Alexander, L. V., & Donat, M. G. (2013). The efficacy of using gridded data to examine extreme rainfall characteristics: A case study for Australia. *International Journal of Climatology*, 33(10), 2376–2387. <https://doi.org/10.1002/joc.3588>
- Kormos, P. R., Luce, C. H., Wenger, S. J., & Berguijs, W. R. (2016). Trends and sensitivities of low streamflow extremes to discharge timing and magnitude in Pacific Northwest mountain streams. *Water Resources Research*, 52(7), 4990–5007. <https://doi.org/10.1002/2015WR018125>
- Kuang, X., Jiao, J. J., Zheng, C., Cherry, J. A., & Li, H. (2020). A review of specific storage in aquifers. *Journal of Hydrology*, 581, 124383. <https://doi.org/10.1016/j.jhydrol.2019.124383>
- Kuss, A. J. M., & Gurdak, J. J. (2014). Groundwater level response in U.S. principal aquifers to ENSO, NAO, PDO, and AMO. *Journal of Hydrology*, 519, 1939–1952. <https://doi.org/10.1016/j.jhydrol.2014.09.069>
- Lafare, A. E. A., Peach, D. W., & Hughes, A. G. (2016). Use of seasonal trend decomposition to understand groundwater behaviour in the Permo-Triassic Sandstone aquifer, Eden Valley, UK. *Hydrogeology Journal*, 24(1), 141–158. <https://doi.org/10.1007/s10040-015-1309-3>
- Lautz, L. K. (2008). Estimating groundwater evapotranspiration rates using diurnal water-table fluctuations in a semi-arid riparian zone. *Hydrogeology Journal*, 16(3), 483–497. <https://doi.org/10.1007/s10040-007-0239-0>

- Li, C., Zwiers, F., Zhang, X., Chen, G., Lu, J., Li, G., et al. (2019). Larger increases in more extreme local precipitation events as climate warms. *Geophysical Research Letters*, 46(12), 6885–6891. <https://doi.org/10.1029/2019GL082908>
- Lopez, H., & Kirtman, B. P. (2019). ENSO influence over the Pacific North American sector: Uncertainty due to atmospheric internal variability. *Climate Dynamics*, 52(9), 6149–6172. <https://doi.org/10.1007/s00382-018-4500-0>
- Maity, R. (2018). Time series analysis. In R. Maity (Ed.), *Statistical methods in hydrology and hydroclimatology* (pp. 305–379). Springer. https://doi.org/10.1007/978-981-10-8779-0_9
- Malmgren, K. A., Neves, C., Gurdak, J. J., Costa, L., & Monteiro, J. P. (2022). Groundwater response to climate variability in Mediterranean type climate zones with comparisons of California (USA) and Portugal. *Hydrogeology Journal*, 30(3), 767–782. <https://doi.org/10.1007/s10040-022-02470-z>
- Mangin, A. (1984). Pour une meilleure connaissance des systèmes hydrologiques à partir des analyses corrélatoire et spectrale. *Journal of Hydrology*, 67(1), 25–43. [https://doi.org/10.1016/0022-1694\(84\)90230-0](https://doi.org/10.1016/0022-1694(84)90230-0)
- Mantua, N. J., & Hare, S. R. (2002). The pacific decadal oscillation. *Journal of Oceanography*, 58(1), 35–44. <https://doi.org/10.1023/A:1015820616384>
- Mao, X., Enot, P., Barry, D. A., Li, L., Binley, A., & Jeng, D.-S. (2006). Tidal influence on behaviour of a coastal aquifer adjacent to a low-relief estuary. *Journal of Hydrology*, 327(1), 110–127. <https://doi.org/10.1016/j.jhydrol.2005.11.030>
- Martins, E. G., Déry, S. J., & Patterson, D. A. (2023). Chapter 15—Fraser River basin. In M. D. Delong, T. D. Jardine, A. C. Benke, & C. E. Cushing (Eds.), *Rivers of north America* (2nd ed., pp. 650–674). Academic Press. <https://doi.org/10.1016/B978-0-12-818847-7.00006-9>
- Massei, N., Dupont, J. P., Mahler, B. J., Laignel, B., Fournier, M., Valdes, D., & Ogier, S. (2006). Investigating transport properties and turbidity dynamics of a karst aquifer using correlation, spectral, and wavelet analyses. *Journal of Hydrology*, 329(1), 244–257. <https://doi.org/10.1016/j.jhydrol.2006.02.021>
- McKee, T., Doesken, N., & Kleist, J. (1993). The relationship of drought frequency and duration to time scales. In *Eighth conference on applied climatology*. Anaheim. Retrieved from <https://climate.colostate.edu/pdfs/relationshipofdroughtfrequency.pdf>
- McMillan, T. C., Rau, G. C., Timms, W. A., & Andersen, M. S. (2019). Utilizing the impact of earth and atmospheric tides on groundwater systems: A review reveals the future potential. *Reviews of Geophysics*, 57(2), 281–315. <https://doi.org/10.1029/2018RG000630>
- Meixner, T., Manning, A. H., Stonestrom, D. A., Allen, D. M., Ajami, H., Blasch, K. W., et al. (2016). Implications of projected climate change for groundwater recharge in the western United States. *Journal of Hydrology*, 534, 124–138. <https://doi.org/10.1016/j.jhydrol.2015.12.027>
- Moore, R. D., Spittlehouse, D. L., Whitfield, P. H., & Stahl, K. (2010). Chapter 3—Weather and climate (66; Compendium of forest hydrology and geomorphology in British Columbia). *Forum for Research and Extension in Natural Resources*. https://www.for.gov.bc.ca/hfd/pubs/docs/lmh/Lmh66/LMH66_ch03.pdf
- Mote, P. W., Hamlet, A. F., Clark, M. P., & Lettenmaier, D. P. (2005). Declining mountain snowpack in Western North America. *Bulletin of the American Meteorological Society*, 86(1), 39–50. <https://doi.org/10.1175/BAMS-86-1-39>
- Mote, P. W., Rupp, D. E., Li, S., Sharp, D. J., Otto, F., Uhe, P. F., et al. (2016). Perspectives on the causes of exceptionally low 2015 snowpack in the western United States. *Geophysical Research Letters*, 43(20), 10980–10988. <https://doi.org/10.1002/2016GL069965>
- Mundhenk, B. D., Barnes, E. A., & Maloney, E. D. (2016). All-season climatology and variability of atmospheric river frequencies over the North Pacific. *Journal of Climate*, 29(13), 4885–4903. <https://doi.org/10.1175/JCLI-D-15-0655.1>
- Murray, J., Ayers, J., & Brookfield, A. (2023). The impact of climate change on monthly baseflow trends across Canada. *Journal of Hydrology*, 618, 129254. <https://doi.org/10.1016/j.jhydrol.2023.129254>
- Neiman, P. J., Ralph, F. M., Wick, G. A., Lundquist, J. D., & Dettinger, M. D. (2008). Meteorological characteristics and overland precipitation impacts of atmospheric rivers affecting the west coast of North America based on eight years of SSM/I satellite observations. *Journal of Hydrometeorology*, 9(1), 22–47. <https://doi.org/10.1175/2007JHM855.1>
- Nott, A. H., Allen, D. M., & Hahm, W. J. (2024). Groundwater responses to Deluge and drought in the Pacific Northwest [Dataset and Code]. *Hydro*. <https://www.hydroshare.org/resource/d77f1c4ff8245d498fa7b924fe028a/>
- Nygren, M., Barthel, R., Allen, D. M., & Giese, M. (2022). Exploring groundwater drought responsiveness in lowland post-glacial environments. *Hydrogeology Journal*, 30(7), 1937–1961. <https://doi.org/10.1007/s10040-022-02521-5>
- O'Brien, T. A., Wehner, M. F., Payne, A. E., Shields, C. A., Rutz, J. J., Leung, L.-R., et al. (2022). Increases in future AR count and size: Overview of the ARTMIP tier 2 CMIP6 experiment. *Journal of Geophysical Research: Atmospheres*, 127(6), e2021JD036013. <https://doi.org/10.1029/2021JD036013>
- Opie, S., Taylor, R. G., Brierley, C. M., Shamsuddoha, M., & Cuthbert, M. O. (2020). Climate–groundwater dynamics inferred from GRACE and the role of hydraulic memory. *Earth System Dynamics*, 11(3), 775–791. <https://doi.org/10.5194/esd-11-775-2020>
- Paltan, H., Waliser, D., Lim, W. H., Guan, B., Yamazaki, D., Pant, R., & Dadson, S. (2017). Global Floods and water availability driven by atmospheric rivers. *Geophysical Research Letters*, 44(20), 10387–10395. <https://doi.org/10.1002/2017GL074882>
- Pawlowicz, R., Di Costanzo, R., Halverson, M., Devred, E., & Johannessen, S. (2017). Advection, surface area, and sediment load of the Fraser river plume under variable wind and river forcing. *Atmosphere-Ocean*, 55(4–5), 293–313. <https://doi.org/10.1080/07055900.2017.1389689>
- Payne, A. E., Demory, M.-E., Leung, L. R., Ramos, A. M., Shields, C. A., Rutz, J. J., et al. (2020). Responses and impacts of atmospheric rivers to climate change. *Nature Reviews Earth and Environment*, 1(3), 143–157. <https://doi.org/10.1038/s43017-020-0030-5>
- Payne, A. E., & Magnusdottir, G. (2014). Dynamics of landfalling atmospheric rivers over the North Pacific in 30 years of MERRA reanalysis. *Journal of Climate*, 27(18), 7133–7150. <https://doi.org/10.1175/JCLI-D-14-00034.1>
- Peterson, T. J., Saft, M., Peel, M. C., & John, A. (2021). Watersheds may not recover from drought. *Science*, 372(6543), 745–749. <https://doi.org/10.1126/science.abd5085>
- Piteau Associates Engineering Ltd. (2012). Hydrogeological investigation for groundwater supply: Miracle valley, B.C. (Project 3131). Retrieved from [https://www.fvrd.ca/assets/Services/Documents/Water-Systems/FINAL%20REPORT%20FOR%20MIRACLE%20VALLEY%20GW%20STUDY%20-%20PITEAU%2004122012%20\(FILED\).pdf](https://www.fvrd.ca/assets/Services/Documents/Water-Systems/FINAL%20REPORT%20FOR%20MIRACLE%20VALLEY%20GW%20STUDY%20-%20PITEAU%2004122012%20(FILED).pdf)
- Prein, A. F., Rasmussen, R. M., Ikeda, K., Liu, C., Clark, M. P., & Holland, G. J. (2017). The future intensification of hourly precipitation extremes. *Nature Climate Change*, 7(1), 48–52. <https://doi.org/10.1038/nclimate3168>
- QGIS Development Team. (2022). QGIS geographic information system (3.26.3) [Computer Software]. *QGIS Association*. Retrieved from <https://qgis.org/en/site/>
- Ralph, F. M., Cordeira, J. M., Neiman, P. J., & Hughes, M. (2016). Landfalling atmospheric rivers, the Sierra Barrier jet, and extreme daily precipitation in Northern California's upper Sacramento river watershed. *Journal of Hydrometeorology*, 17(7), 1905–1914. <https://doi.org/10.1175/JHM-D-15-0167.1>
- Ralph, F. M., Dettinger, M. D., Cairns, M. M., Galarneau, T. J., & Eylander, J. (2018). Defining “atmospheric river”: How the glossary of meteorology helped resolve a debate. *Bulletin of the American Meteorological Society*, 99(4), 837–839. <https://doi.org/10.1175/BAMS-D-17-0157.1>

- Rathay, S. Y., Allen, D. M., & Kirste, D. (2018). Response of a fractured bedrock aquifer to recharge from heavy rainfall events. *Journal of Hydrology*, 561, 1048–1062. <https://doi.org/10.1016/j.jhydrol.2017.07.042>
- R Core Team. (2022). R: A language and environment for statistical computing [Computer Software]. *R Foundation for Statistical Computing*. Retrieved from <https://www.R-project.org/>
- Ricketts, B. D. (1998). *Groundwater flow beneath the Fraser River delta, British Columbia; a preliminary model (geological survey of Canada Bulletin)* (Vol. 525, pp. 241–255). Geological Survey of Canada. <https://doi.org/10.4095/210047>
- Ricketts, B. D. (2000). *Modelling of groundwater flow in the Fraser River delta and brookwood aquifer geological survey of Canada Bulletin* (Vol. 552, pp. 103–130). Geological Survey of Canada. <https://doi.org/10.4095/211545>
- Roesch, A., & Schmidbauer, H. (2018). WaveletComp: Computational wavelet analysis (R package version 1.1) [Computer Software]. <https://CRAN.R-project.org/package=WaveletComp>
- Rust, W., Holman, I., Bloomfield, J., Cuthbert, M., & Corstanje, R. (2019). Understanding the potential of climate teleconnections to project future groundwater drought. *Hydrology and Earth System Sciences*, 23(8), 3233–3245. <https://doi.org/10.5194/hess-23-3233-2019>
- Rutz, J. J., Shields, C. A., Lora, J. M., Payne, A. E., Guan, B., Ullrich, P., et al. (2019). The atmospheric river tracking method intercomparison project (ARTMIP): Quantifying uncertainties in atmospheric river climatology. *Journal of Geophysical Research: Atmospheres*, 124(24), 13777–13802. <https://doi.org/10.1029/2019JD030936>
- Rutz, J. J., Steenburgh, W. J., & Ralph, F. M. (2014). Climatological characteristics of atmospheric rivers and their inland penetration over the Western United States. *Monthly Weather Review*, 142(2), 905–921. <https://doi.org/10.1175/MWR-D-13-00168.1>
- Sang, Y.-F. (2013). A review on the applications of wavelet transform in hydrology time series analysis. *Atmospheric Research*, 122, 8–15. <https://doi.org/10.1016/j.atmosres.2012.11.003>
- Schuler, P., Campanyà, J., Moe, H., Doherty, D., Williams, N. H., & McCormack, T. (2022). Mapping the groundwater memory across Ireland: A step towards a groundwater drought susceptibility assessment. *Journal of Hydrology*, 612, 128277. <https://doi.org/10.1016/j.jhydrol.2022.128277>
- Schuler, P., Duran, L., Johnston, P., & Gill, L. (2020). Quantifying and numerically representing recharge and flow components in a karstified carbonate aquifer. *Water Resources Research*, 56(11), e2020WR027717. <https://doi.org/10.1029/2020WR027717>
- Scibek, J., & Allen, D. M. (2005). *Numerical groundwater flow model of the Abbotsford-Sumas aquifer, central Fraser Lowland of BC, Canada and Washington state, US (prepared for Environment Canada)*. Simon Fraser University. Retrieved from https://www.sfu.ca/personal/dallen/AB_Modeling_Report_Final.pdf
- Seager, R., Harmik, N., Robinson, W. A., Kushnir, Y., Ting, M., Huang, H.-P., & Velez, J. (2005). Mechanisms of ENSO-forcing of hemispherically symmetric precipitation variability. *Quarterly Journal of the Royal Meteorological Society*, 131(608), 1501–1527. <https://doi.org/10.1256/qj.04.96>
- Shao, J., Si, B., & Jin, J. (2018). Extreme precipitation years and their occurrence frequency regulate long-term groundwater recharge and transit time. *Vadose Zone Journal*, 17(1), 180093–180099. <https://doi.org/10.2136/vzj2018.04.0093>
- Sharma, A. R., & Déry, S. J. (2020). Contribution of atmospheric rivers to annual, seasonal, and extreme precipitation across British Columbia and southeastern Alaska. *Journal of Geophysical Research: Atmospheres*, 125(9), e2019JD031823. <https://doi.org/10.1029/2019JD031823>
- Siirila-Woodburn, E. R., Dennedy-Frank, P. J., Rhoades, A., Vahmani, P., Maina, F., Hatchett, B., et al. (2023). The role of atmospheric rivers on groundwater: Lessons learned from an extreme wet year. *Water Resources Research*, 59(6), e2022WR033061. <https://doi.org/10.1029/2022WR033061>
- Sorensen, J. P. R., Davies, J., Ebrahim, G. Y., Lindle, J., Marchant, B. P., Ascott, M. J., et al. (2021). The influence of groundwater abstraction on interpreting climate controls and extreme recharge events from well hydrographs in semi-arid South Africa. *Hydrogeology Journal*, 29(8), 2773–2787. <https://doi.org/10.1007/s10040-021-02391-3>
- Spry, C. M., Kohfeld, K. E., Allen, D. M., Dunkley, D., & Lertzman, K. (2014). Characterizing pineapple express storms in the lower mainland of British Columbia, Canada. *Canadian Water Resources Journal / Revue Canadienne Des Ressources Hydrauliques*, 39(3), 302–323. <https://doi.org/10.1080/07011784.2014.942574>
- Sun, Q., Miao, C., Duan, Q., Ashouri, H., Sorooshian, S., & Hsu, K.-L. (2018). A review of global precipitation data sets: Data sources, estimation, and intercomparisons. *Reviews of Geophysics*, 56(1), 79–107. <https://doi.org/10.1002/2017RG000574>
- Sun, Q., Zhang, X., Zwiers, F., Westra, S., & Alexander, L. V. (2021). A Global, continental, and regional analysis of changes in extreme precipitation. *Journal of Climate*, 34(1), 243–258. <https://doi.org/10.1175/JCLI-D-19-0892.1>
- Sutanto, S. J., & Van Lanen, H. A. J. (2022). Catchment memory explains hydrological drought forecast performance. *Scientific Reports*, 12(1), 2689. <https://doi.org/10.1038/s41598-022-06553-5>
- Tan, Y., Yang, S., Zwiers, F., Wang, Z., & Sun, Q. (2022). Moisture budget analysis of extreme precipitation associated with different types of atmospheric rivers over western North America. *Climate Dynamics*, 58(3), 793–809. <https://doi.org/10.1007/s00382-021-05933-3>
- Taylor, R. G., Todd, M. C., Kongola, L., Maurice, L., Nahozya, E., Sanga, H., & MacDonald, A. M. (2013). Evidence of the dependence of groundwater resources on extreme rainfall in East Africa. *Nature Climate Change*, 3(4), 374–378. <https://doi.org/10.1038/nclimate1731>
- Teuling, A. J., Van Loon, A. F., Seneviratne, S. I., Lehner, I., Aubinet, M., Heinesch, B., et al. (2013). Evapotranspiration amplifies European summer drought. *Geophysical Research Letters*, 40(10), 2071–2075. <https://doi.org/10.1029/grl.50495>
- Thomas, B. F., Behrangi, A., & Famiglietti, J. S. (2016). Precipitation intensity effects on groundwater recharge in the southwestern United States. *Water*, 8(3), 90. <https://doi.org/10.3390/w8030090>
- Toll, N. J., & Rasmussen, T. C. (2007). Removal of barometric pressure effects and earth tides from observed water levels. *Ground Water*, 45(1), 101–105. <https://doi.org/10.1111/j.1745-6584.2006.00254.x>
- Torrence, C., & Compo, G. P. (1998). A practical guide to wavelet analysis. *Bulletin of the American Meteorological Society*, 79(1), 61–78. [https://doi.org/10.1175/1520-0477\(1998\)079<0061:APGTWA>2.0.CO;2](https://doi.org/10.1175/1520-0477(1998)079<0061:APGTWA>2.0.CO;2)
- Vallejo-Bernal, S. M., Wolf, F., Boers, N., Traxl, D., Marwan, N., & Kurths, J. (2023). The role of atmospheric rivers in the distribution of heavy precipitation events over North America. *Hydrology and Earth System Sciences*, 27(14), 2645–2660. <https://doi.org/10.5194/hess-27-2645-2023>
- Van Lanen, H. A. J. (2006). Drought propagation through the hydrological cycle. Climate variability and change: Hydrological impacts. In *Proceedings of the fifth FRIEND world conference, Havana, Cuba, november* (Vol. 308, pp. 122–127). IAHS Publ.
- Van Lanen, H. A. J., Wanders, N., Tallaksen, L. M., & Van Loon, A. F. (2013). Hydrological drought across the world: Impact of climate and physical catchment structure. *Hydrology and Earth System Sciences*, 17(5), 1715–1732. <https://doi.org/10.5194/hess-17-1715-2013>
- Van Loon, A. F. (2015). Hydrological drought explained. *WIREs Water*, 2(4), 359–392. <https://doi.org/10.1002/wat2.1085>
- Velasco, E. M., Gurdak, J. J., Dickinson, J. E., Ferré, T. P. A., & Corona, C. R. (2017). Interannual to multidecadal climate forcings on groundwater resources of the U.S. West Coast. *Journal of Hydrology: Regional Studies*, 11, 250–265. <https://doi.org/10.1016/j.ejrh.2015.11.018>

- Vicente-Serrano, S. M., López-Moreno, J. I., Gimeno, L., Nieto, R., Morán-Tejeda, E., Lorenzo-Lacruz, J., et al. (2011). A multiscale global evaluation of the impact of ENSO on droughts. *Journal of Geophysical Research*, 116(D20), D20109. <https://doi.org/10.1029/2011JD016039>
- Wang, H. F. (2020). Groundwater storage in confined aquifers. The groundwater project. Retrieved from <https://books.gw-project.org/groundwater-storage-in-confined-aquifers>
- Wang, S., Ma, X., Zhou, S., Wu, L., Wang, H., Tang, Z., et al. (2023). Extreme atmospheric rivers in a warming climate. *Nature Communications*, 14(1), 3219. <https://doi.org/10.1038/s41467-023-38980-x>
- Wang, W., Ertsen, M. W., Svoboda, M. D., & Hafeez, M. (2016). Propagation of drought: From meteorological drought to agricultural and hydrological drought. *Advances in Meteorology*, 2016, 1–5. <https://doi.org/10.1155/2016/6547209>
- Wendt, D. E., Van Loon, A. F., Bloomfield, J. P., & Hannah, D. M. (2020). Asymmetric impact of groundwater use on groundwater droughts. *Hydrology and Earth System Sciences*, 24(10), 4853–4868. <https://doi.org/10.5194/hess-24-4853-2020>
- Winter, T. C. (1999). Relation of streams, lakes, and wetlands to groundwater flow systems. *Hydrogeology Journal*, 7(1), 28–45. <https://doi.org/10.1007/s100400050178>
- Witt, A., & Malamud, B. D. (2013). Quantification of long-range persistence in geophysical time series: Conventional and benchmark-based improvement techniques. *Surveys in Geophysics*, 34(5), 541–651. <https://doi.org/10.1007/s10712-012-9217-8>
- Wittenberg, H., Aksoy, H., & Miegel, K. (2019). Fast response of groundwater to heavy rainfall. *Journal of Hydrology*, 571, 837–842. <https://doi.org/10.1016/j.jhydrol.2019.02.037>
- WLRS. (2023). Ground water aquifers—Ministry of water, Land and resource stewardship (WLRS)—Aquifer information. Retrieved from <https://catalogue.data.gov.bc.ca/dataset/099d69c5-1401-484d-9e19-c121ccb7977c>
- WLRS. (2024). Water rights databases—Province of British Columbia. Province of British Columbia. Retrieved from <https://www2.gov.bc.ca/gov/content/environment/air-land-water/water/water-licensing-rights/water-licences-approvals/water-rights-databases>
- Woessner, W. W. (2000). Stream and fluvial plain ground water interactions: Rescaling hydrogeologic thought. *Ground Water*, 38(3), 423–429. <https://doi.org/10.1111/j.1745-6584.2000.tb00228.x>
- WSC. (2023). Daily discharge and stage for Fraser River at mission (08MH024) [BC]—Water level and flow—Environment Canada—Water Survey of Canada. Retrieved from https://wateroffice.ec.gc.ca/report/historical_e.html?stn=08MH024
- Xiong, Y., & Ren, X. (2021). Influences of atmospheric rivers on north pacific winter precipitation: Climatology and dependence on ENSO condition. *Journal of Climate*, 34(1), 277–292. <https://doi.org/10.1175/JCLI-D-20-0301.1>
- Yin, J., Medellín-Azuara, J., & Escrivá-Bou, A. (2022). Groundwater levels hierarchical clustering and regional groundwater drought assessment in heavily drafted aquifers. *Hydrology Research*, 53(7), 1031–1046. <https://doi.org/10.2166/nh.2022.048>
- Zhu, Y., & Newell, R. E. (1998). A proposed algorithm for moisture fluxes from atmospheric rivers. *Monthly Weather Review*, 126(3), 725–735. [https://doi.org/10.1175/1520-0493\(1998\)126<0725:APAFMF>2.0.CO;2](https://doi.org/10.1175/1520-0493(1998)126<0725:APAFMF>2.0.CO;2)